May 2017

Analysis of Zinc Oxide Thin Films Synthesized By Sol-Gel via Spin Coating

Jon Carl Wolgamott
University of Wisconsin-Milwaukee

ANALYSIS OF ZINC OXIDE THIN FILMS SYNTHESIZED BY SOL-GEL VIA SPIN COATING

by

Jon Carl Wolgamott

A Thesis Submitted in

Partial Fulfillment of the

Requirements for the Degree of

Master of Science

in Engineering

at

The University of Wisconsin-Milwaukee

May 2017

ABSTRACT

ANALYSIS OF ZINC OXIDE THIN FILMS SYNTHESIZED BY SOL-GEL VIA SPIN COATING

by

Jon Carl Wolgamott

The University of Wisconsin-Milwaukee, 2016
Under the Supervision of Professor Nidal Abu-Zahra

Transparent conductive oxides are gaining an increasingly important role in optoelectronic devices such as solar cells. Doped zinc oxide is a candidate as a low cost and nontoxic alternative to tin doped indium oxide. Lab results have shown that both n-type and p-type zinc oxide can be created on a small scale. This can allow zinc oxide to be used as either an electrode as well as a buffer layer to increase efficiency and protect the active layer in solar cells.

Sol-gel synthesis is emerging as a low temperature, low cost, and resource efficient alternative to producing transparent conducting oxides such as zinc oxide. For sol-gel derived zinc oxide thin films to reach their potential, research in this topic must continue to optimize the known processing parameters and expand to new parameters to tighten control and create novel processing techniques that improve performance.

The processing parameters of drying and annealing temperatures as well as cooling rate were analyzed to see their effect on the structure of the prepared zinc oxide thin films. There were also preliminary tests done to modify the sol-gel process to include silver as a dopant to produce a p-type thin film. The results from this work show that the pre- and post- heating temperatures as well as the cooling rate all play their own unique role in the crystallization of the film. Results from silver doping show that more work needs to be done to create a sol-gel derived p-type zinc oxide thin film.

I would like to thank my advisor, Dr. Nidal Abu-Zahra for allowing me the freedom to choose and study this important topic. Also for providing encouragement and motivation when times became difficult.

I would also like to thank my defense members Dr. Steve Hardcastle and Dr. Junjie Niu for their help throughout my research on analyzing the results from characterization.

Additionally, I would like to thank Reed Heintzkill, Karl Flanagan-Morris, Eric Ruzicka, and Nadia Rabbani for their contributions to various stages of my research.

Finally, above all else, I would like to send a special thank you to my mother, Lonnie Wolgamott, who without her love and support, this would not be possible, for always believing in me and allowing me to achieve my dreams.

TABLE OF CONTENTS

LIST OF FIGURES

Chapter 1: Introduction

Transparent conductive oxides

Transparent conductive oxides (TCOs) are important for devices such as LCDs, LEDs, and touch panels (D.J. Rogers, 2010) (H. Zeng, 2009) (J. Hong, 2012). These types of devices require a material that can transport charge carriers but also allow photons from the visible light spectrum to pass through. For this reason, it is desired that TCOs have a band gap between 3 and 4 eV, resistivity lower than 10^{-3} Ω cm, visible range transmittance greater than 80% and a charge carrier concentration greater than 10^{20} cm^{-3} (Minami, 2005) (Yanli Liu, 2013).

Most research being performed on TCOs are on n-type semiconductors and these types of materials make up virtually all the TCOs used in production (Minami, 2005). Research on p-type TCOs started back in 1993 (H. Sato, 1993) and there has been continued research on this topic throughout the years (J. Tate, 2002). Despite this continued interest in publication, there are currently no p-type semiconductors that are suitable to be used as TCOs.

Among TCOs, the most widely used is tin doped indium oxide (ITO) (Stadler, 2012). However, ITO does not have practical scalability as indium, a scarce earth element, has a limited supply, is costly, and toxic making it undesirable to work with on a large scale. Furthermore, an extensive literature review by Minami (Minami, 2005) shows the resistivity of ITO thin films have seemingly plateaued over recent years. There have been other TCOs that show potential for replacing ITO, including Zinc Oxide (ZnO).

Zinc Oxide

ZnO is a widely-used material. In powder form, it can be found as an additive in food and a wide range of materials such as rubber, cement, and lubricants (A. Hernandez Battez, 2008). It is a white pigment that is used in paint, ointments, sunscreen, and toothpastes. This is due to the U.S. Food and Drug Administration including ZnO on the list of substances generally recognized as safe (GRAS). Additionally, research has begun in the use of ZnO in the use inside optoelectronic devices.

ZnO occurs naturally as a rare mineral, Zincite; however, for most applications ZnO must be produced synthetically for specific applications. The Wurtzite structure is the more thermodynamically favorable crystal structure for ZnO as depicted in Figure 1. This is a hexagonal close packed structure with the zinc and oxygen atoms resting at tetrahedral sites with a space group of $C^4_{6v} = p6_3mc$ (Wen-Jun Li, May 1999). The unit cell of this structure has two formula units and exhibits two types of low-index surfaces: polar surfaces $(00\bar{1})$ (O terminated) and (001) (Zn terminated) and non-polar surfaces (100) as well as C_{6v} symmetric surfaces parallel to the c-axis (perpendicular to the surface).

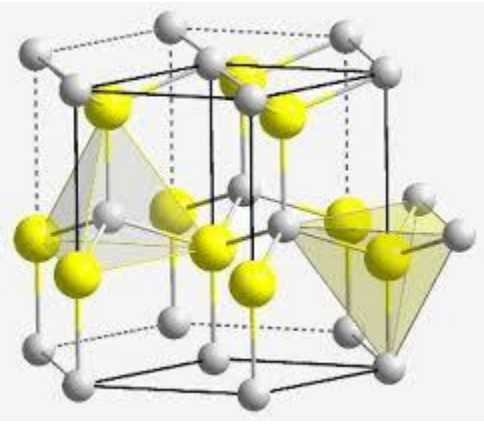

Figure 1: Image depicting Zinc Oxide hexagonal wurtzite structure. (What is Zinc oxide, n.d.)

ZnO is a II-VI semiconductor that has a wide range of unique properties. It has a reported direct and wide band gap of 3.37 eV at room temperature (Thomas, 1960) (A. Mang, 1995) (D. C. Reynolds, 1999) (Y. Chen, 1998). This is within the desired range of 3-4 eV for TCOs and allows for the use of optoelectronic devices utilizing the blue to UV region of the light spectrum. There has been research done on p-n homojunctions (A. Tsukazaki, 2005) (Y.R. Ryu W. K., 2000) (L.J. Mandalapu, 2006) (S. Chu, 2008) but these devices suffer from stability and reproducibility issues.

It has a large free-exciton binding energy of 60 meV (Thomas, 1960) (A. Mang, 1995) (D. C. Reynolds, 1999) (Y. Chen, 1998) (V. Srikant, 1998) (D.C. Reynolds, 1996) (D.M. Bagnall, 1997), which signifies that efficient excitonic emission in ZnO is possible at room temperature. This is good for optical devices that rely on excitonic effects since the oscillator strength of electrons is greater than the strength of direct electron-hole transitions in direct band gap semiconductors such as gallium nitride (GaN) (Yu, 2010).

When a voltage is applied to a piezoelectric material, deformation of the crystal occurs. The reverse is also true which is why piezoelectric materials have gained interest recently as they produce a current when a load is applied to them. These are typically used in sensors, transducers, and actuators. The hexagonal wurtzite structure of ZnO has a low symmetry and a large electromechanical coupling gives it strong piezoelectric and pyroelectric properties (T. Yamamoto, 2008) (Ylilammi, 2003) (R. Ondo-Ndong, 2003) (J.G.E. Gardeniers, 1998).

The typical n-type conductivity displayed by ZnO makes it ideal for use in applications such as vacuum fluorescent displays and field emission displays. This is due to ZnO's strength in the green-white region. It has been recorded of having an emission spectrum with a peak at 495 nm and a broad half-width of 0.4eV (S. Shionoya, 2006). It is believed that the reason for this

luminescence is the native defeats of oxygen vacancies and zinc interstitials. However, this has not yet been confirmed.

ZnO is often used as a gas sensor due to its sensitivity when exposed to various gases resulting in a change of conductivity. It has been used to detect ammonia gas (M.S. Wagh, 2006), ethanol vapor (Rao, 2000), formaldehyde (H. Me, 2014), and a wide range of other gases. The high thermal conductivity of ZnO (D. I. Florescu, 2001) (Ü. Özgür, 2006) makes it desirable as an additive in rubber and a substrate for the growth of GaN. Compared to GaN, large single crystals of ZnO are easily made and commercially available.

The ability to etch semiconductors allows for production of a wider range of integrated electronics and optoelectronic devices. Wet etching is a cheap processing method and ZnO has shown the ability to be etched with acidic, alkaline, and a mixture of other solutions (Y. Wang, 2014) (A.A. Ralib, 2016). Radiation hardness, is another parameter that can open up possibilities for a material's use in high altitude or space applications. ZnO has been reported to have a high radiation hardness (D. C. Look, 1999) (F. Tuomisto, 2005).

Doping of Zinc Oxide

There is a disproportionate amount of n-type produced ZnO films to p-type ZnO films. Part of this inequality of production is due to the native defects that occur in ZnO depicted in Figure 2. Hole killer defects such as zinc interstitial and oxygen vacancies have low formation energies and occur more readily. Electron killer defects such as oxygen interstitial and zinc vacancies have higher formation energy and occur less frequently; this results in ZnO being a native n-type material under most processing conditions (K. Yim, 2017) (C. H. Park, 2002) (S. B. Zhang, 2001) (Yanli Liu, 2013).

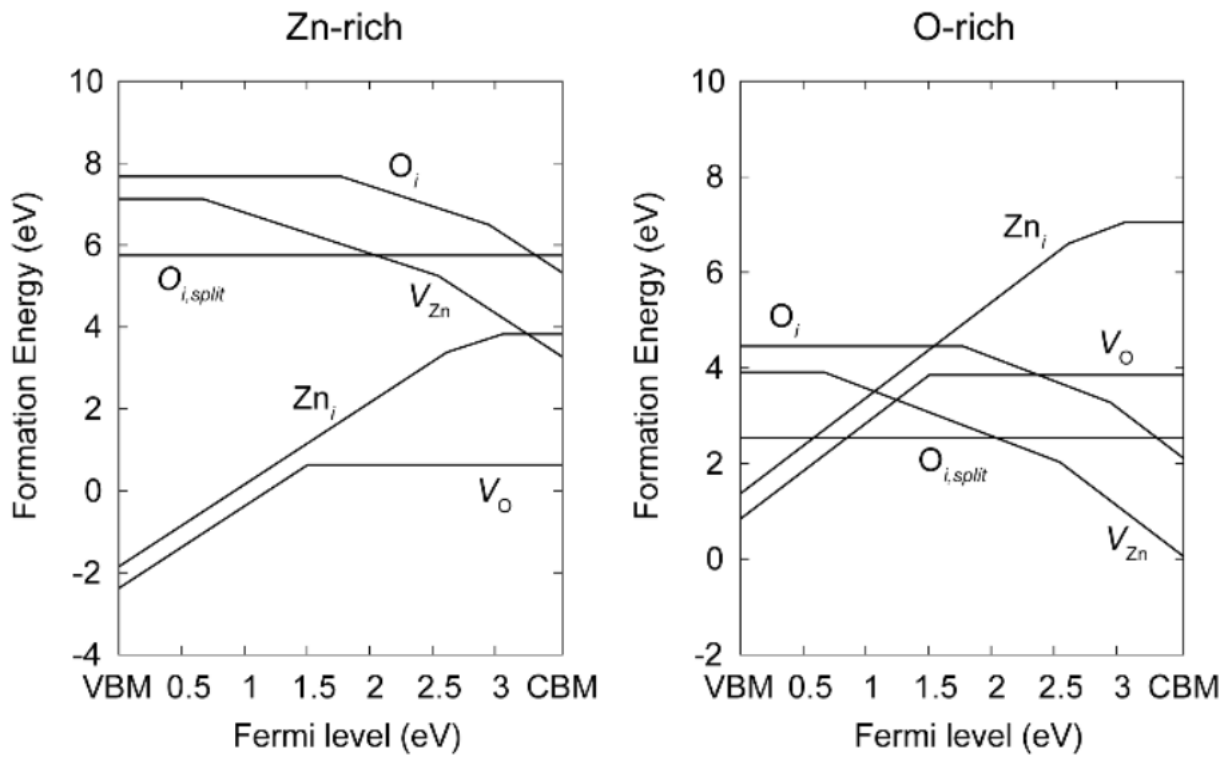

Figure 2: Image showing the formation energies of various intrinsic defects in ZnO over a range of fermi levels for both Zn and O rich conditions (K. Yim, 2017)

The most popular elements doped with ZnO are the group IIIA elements such as aluminum, gallium, and indium. Some of these devices have recently come close to matching the conductivity of ITO (M. Mickan, 2016) (H.S. Chin, 2016). However, ZnO thin films doped with these impurities will only reinforce the n-type nature of ZnO. Figure 3 demonstrates that for a wide range of conditions the group IIIA elements are very stable at zinc substitution sites (K. Yim, 2017). By replacing zinc with these elements will result in an additional electron in the valance band, adding to the negative charge.

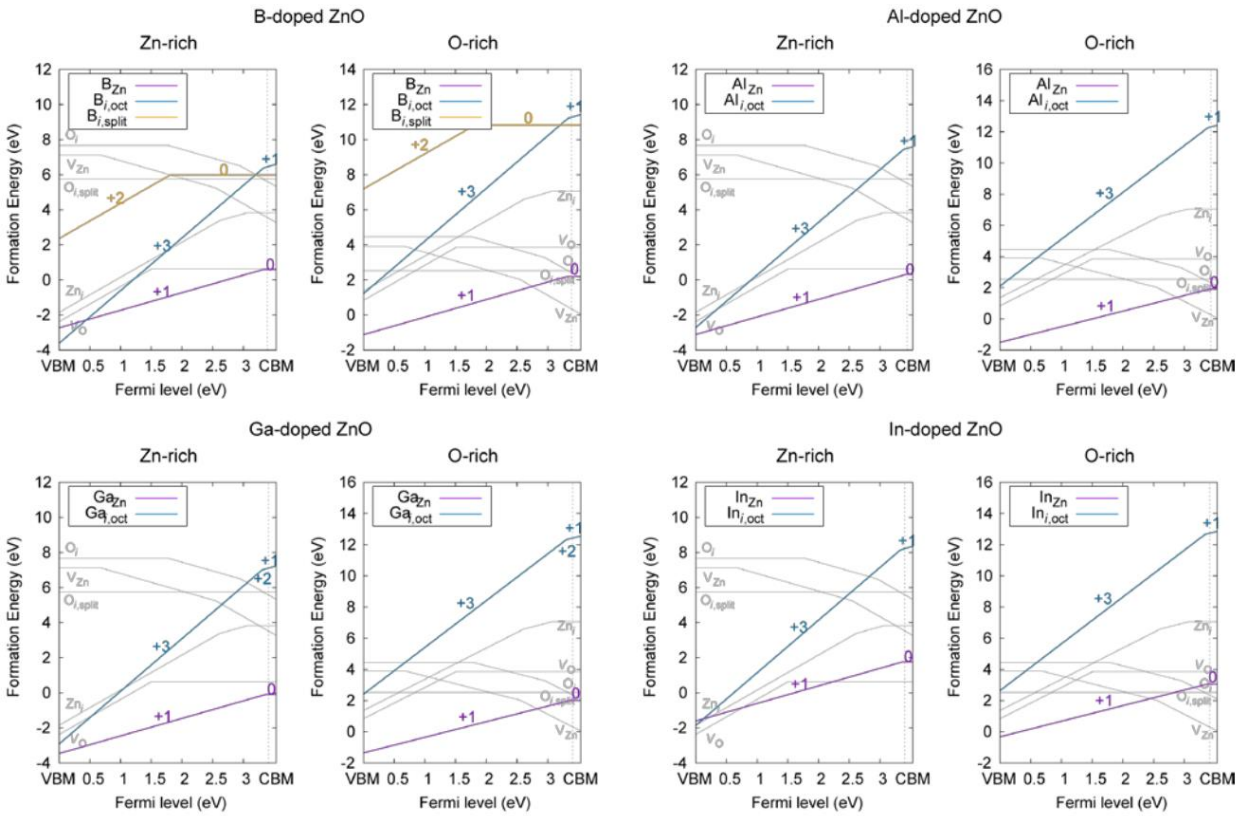

Figure 3: Formation energies of various intrinsic and group IIIA element extrinsic defects in ZnO over a range of fermi levels for both Zn and O rich conditions (K. Yim, 2017)

A similar effect occurs for group VII elements. Figure 4 shows that these elements have a low oxygen substitution formation energy and are stable over a wide range of conditions. This again will add more electrons, reinforcing the n-type charge. Producing n-type ZnO thin films that have a high transparency and a low resistivity is a good step towards replacing ITO.

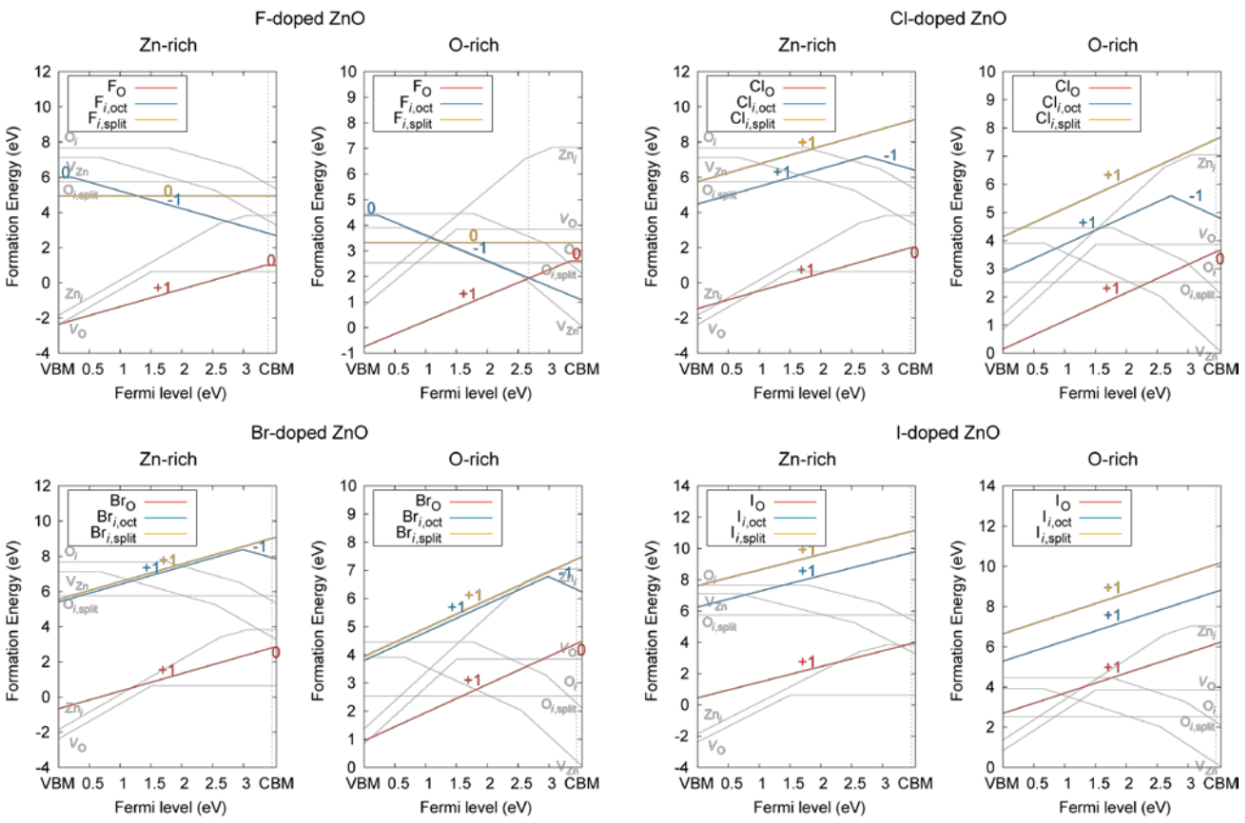

Figure 4: Formation energies of various intrinsic and group VII element extrinsic defects in ZnO over a range of fermi levels for both Zn and O rich conditions (K. Yim, 2017)

P-type doping of Zinc Oxide

Doped ZnO thin films offer the potential for a low cost, low toxicity TCO. Like all TCOs currently in production, ZnO thin films have been mostly limited to n-type doping. If a p-type ZnO TCO could be produced, this would allow for a whole list of possibilities. This could help optoelectronic devices achieve greater efficiencies. The ZnO thin films could be used for either electrode in solar cell devises. This would allow for inverted or even completely transparent solar cells.

There are several challenges to face when attempting to make a p-type ZnO material. Difficulties such as low solubility of the dopant, compensation of low energy, hole killer native defects, deep impurity levels, and structural bistability (C. H. Park, 2002). There have been

reports achieving p-type doped ZnO thin films (M. Joseph, 1999) (Y.R. Ryu S. Z., 2000) (Y. Yan S. Z., 2001); however, these typically require novel processing techniques such as co-doping or nonequilibrium growth conditions to ensure that the desired dopant impurity remains in the final thin film. Reproducibility of these results has proven difficult.

Group VA elements such as nitrogen, phosphorus, and arsenic are common in research attempting to create a p-type ZnO thin film. Their location on the periodic table shows that if they were to form substitutionally with oxygen they would effectively act as an electron killer defect. However, as Figure 5 demonstrates, for most of these elements, the more favorable formation is substitutional with zinc.

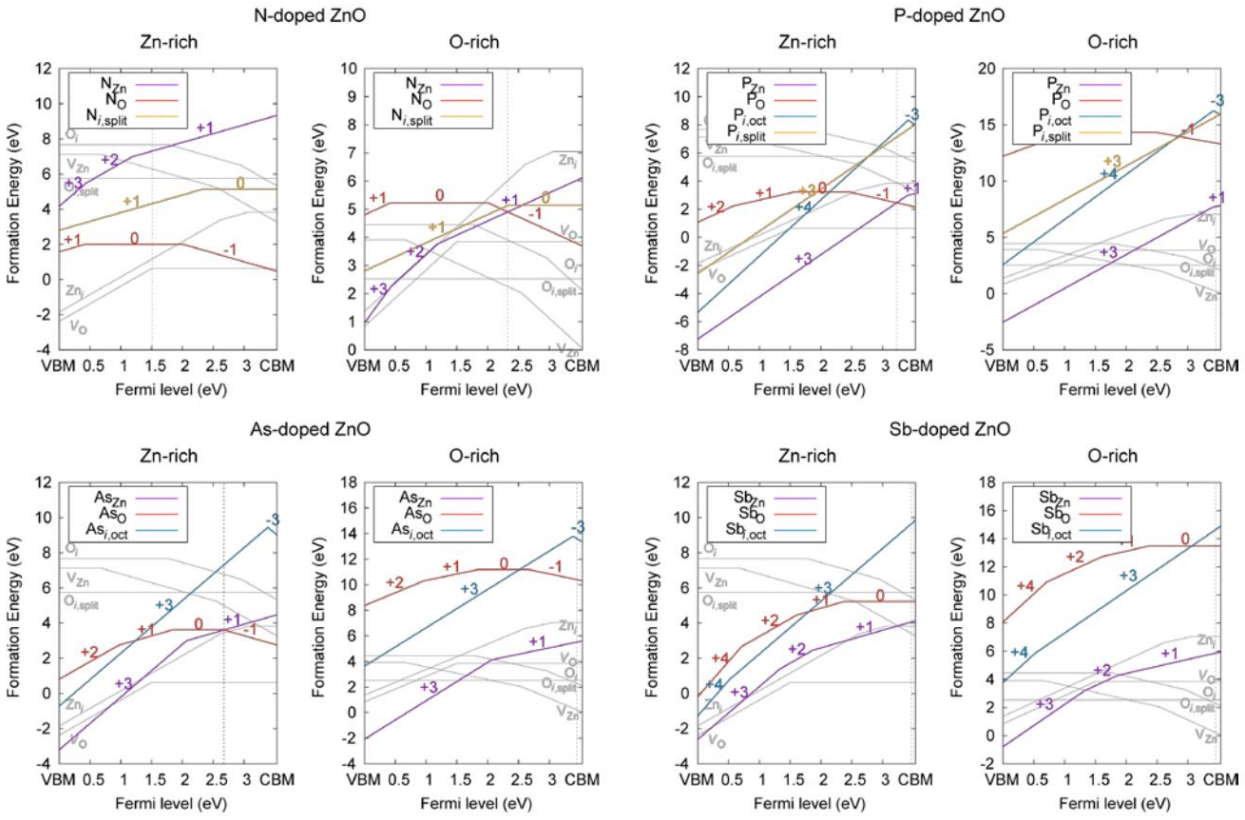

Figure 5: Formation energies of various intrinsic and group VA element extrinsic defects in ZnO over a range of fermi levels for both Zn and O rich conditions (K. Yim, 2017)

The figure also shows that the formation energy is low for nitrogen substituting for oxygen under zinc rich conditions. Nitrogen substituting for oxygen is also a much shallower acceptor than phosphorus or arsenic (C. H. Park, 2002). The measured bond length between nitrogen atoms and the next closest atom is 1.88Å. This is very close to the Zn-O bond length of 1.93Å. For comparison, the bond length for phosphorus and arsenic impurities are 2.18Å and 2.23Å respectively. The smaller the difference is the less strain the defect will put on the crystal lattice. This will not only lower the formation energy, but will suppress the chance of hole killer defects forming to compensate.

Group IA elements lithium, sodium, and potassium have one less electron in their valance band than zinc. If they were to form substitutionally with zinc this could lead to a p-type doped ZnO thin film. Yim et al's (K. Yim, 2017) first principle calculations on the formation of intrinsic and extrinsic defects, shown in Figure 6, indicate that doping with group IA elements may not be so straight forward.

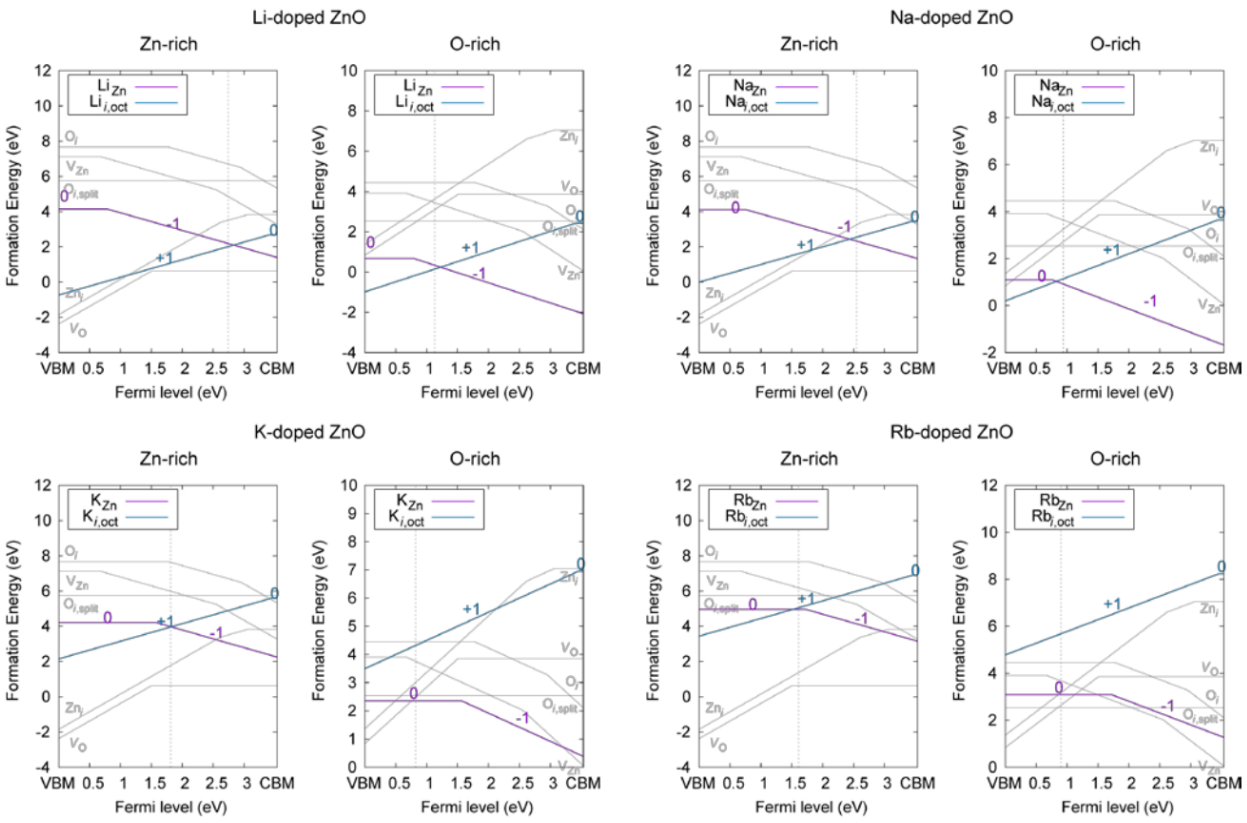

Figure 6: Formation energies of various intrinsic and group IA element extrinsic defects in ZnO over a range of fermi levels for both Zn and O rich conditions (K. Yim, 2017)

As Figure 6 shows, depending on the processing conditions, group IA elements may favor interstitial formation over zinc substitution. This would result in the dopant acting as a hole killer rather than an electron killer. Among the group IA elements, lithium has the smallest difference in bond length between the impurity atom and its nearest neighbor of 2.03Å. This is still a larger difference than that of nitrogen.

Based on first principle calculation done by C.H. Park et al, nitrogen appears to be the most promising although not ideal. The reports that have shown p-type formation from nitrogen doping had to get creative with their processing techniques. This added difficulty, could add to the cost of production and ultimately drive away interest. The analysis done on group IA and VA elements is detailed, however; it does ignore another potential group.

The group IB elements of copper, silver, and gold do not draw as much interest as their group IA and VA counterparts. This does seem a bit surprising as they lie to the left of zinc on the periodic table. This would mean a substitution with zinc would result in an electron killer defect. Although they might be considered expensive, copper and silver would be cheaper alternative to other elements that have been used as dopants. Finally, they are known for their unique conductivity.

Figures 7 and 8 show the formation energies for defects of copper, silver, and gold doped ZnO. These figures, along with a detailed first principle calculation done by Yan et al (Y. Yan M. A.-J., 2006) show that under oxygen rich conditions group IB elements have a low formation energy for zinc substitution formation. This same oxygen rich condition also suppresses the formation of native hole killer defects, thus increasing the possibility for a p-type doped ZnO thin film.

Copper and silver offer a better route to reproducible p-type ZnO thin films. Nitrogen doping is only favorable in zinc rich conditions. This increases the likelihood of hole killer defects forming to compensate. To adjust for this, novel and nonequilibrium processing techniques must be used. This increased difficulty increases processing costs and reduces reproducibility.

First principle calculations show that copper and silver have stable zinc substitution formation under oxygen rich conditions. Under these conditions native hole killing defects are less likely to form to compensate for the extrinsic defeats. This indicates that equilibrium or near equilibrium processing techniques can be used. This should lessen processing costs and allow for greater reproducibility.

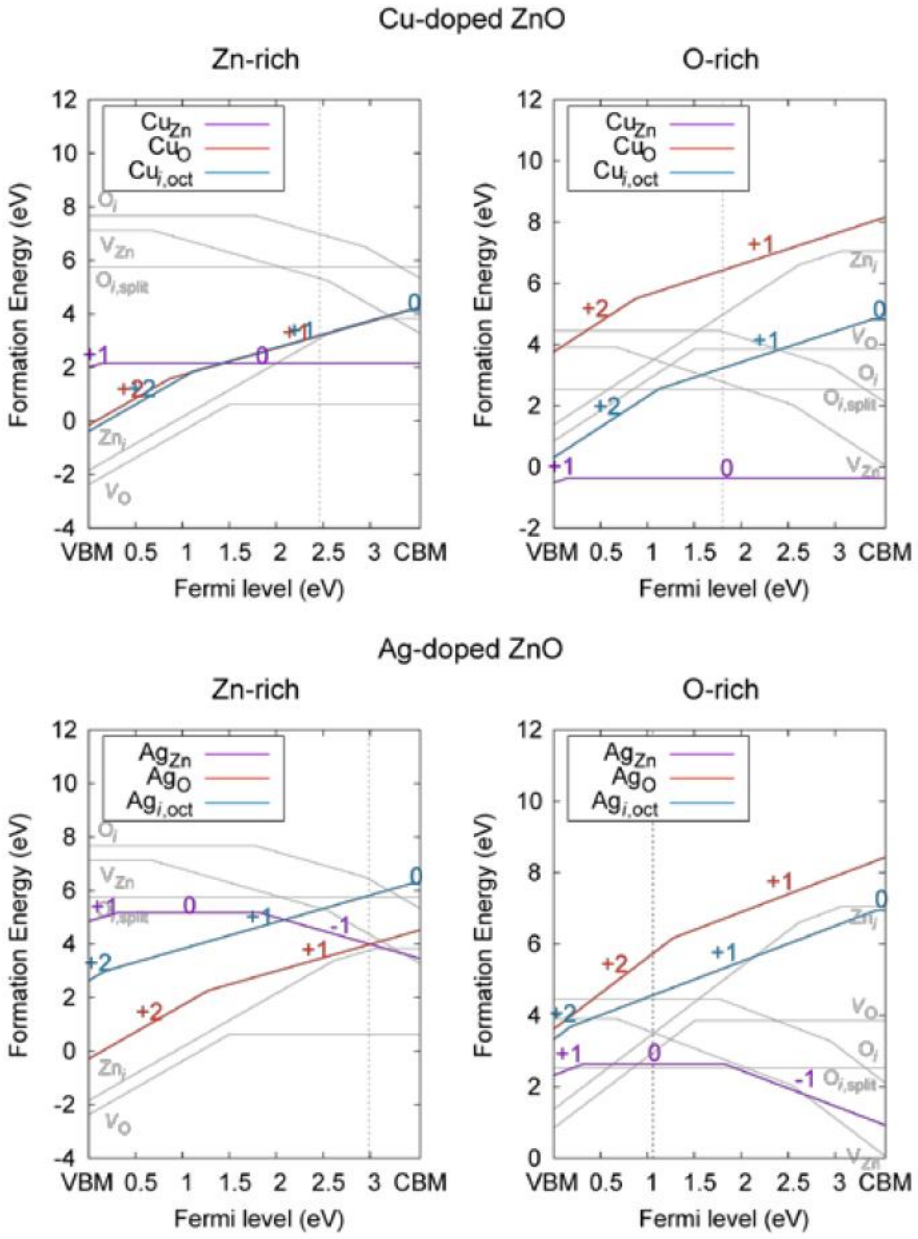

Figure 7: Formation energies of various intrinsic as well as cooper and silver extrinsic defects in ZnO over a range of fermi levels for both Zn and O rich conditions (K. Yim, 2017)

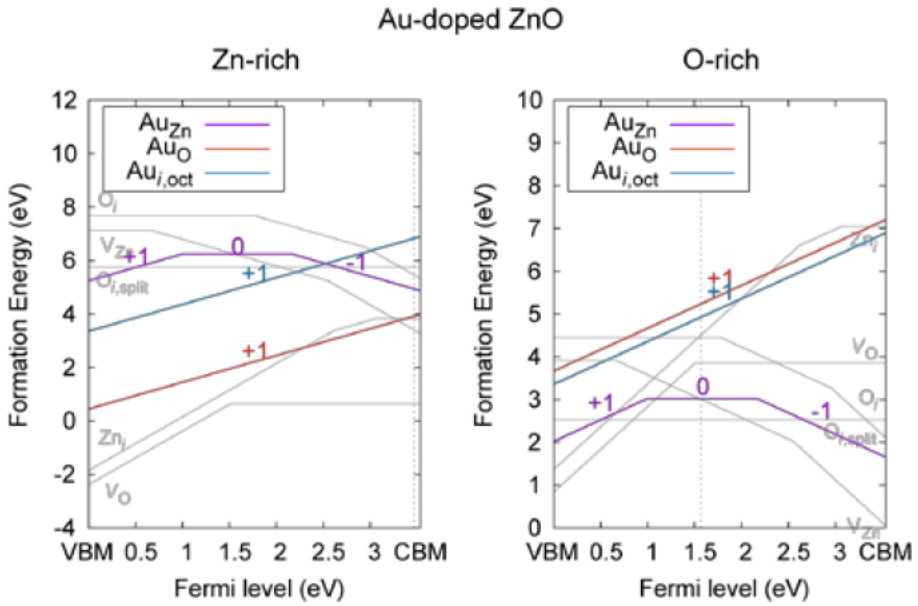

Figure 8: Formation energies of various intrinsic and gold extrinsic defects in ZnO over a range of fermi levels for both Zn and O rich conditions (K. Yim, 2017)

Thin Film Processing

There are many applications for thin film processing. The most popular for ZnO thin films are pulsed laser deposition (PLD), chemical vapor deposition (CVD), metalorganic chemical vapor deposition (MOCVD) and molecular-beam epitaxy (Walle, 2009). These processing parameters allow for the production of high performance ZnO materials. Recently, new processing techniques have popularized, such as chemical spray pyrolysis, screen printing, electrochemical deposition, and sol-gel synthesis with the later offering a low cost, resource efficient process.

Pulsed Laser Deposition

Pulsed laser deposition (PLD) rose in popularity during the late 1980's when it proved successful in growing in-situ epitaxial high-temperature superconducting films (T. Venkatesan, 1988). It provided several advantages such as stoichiometric transfer, excited oxidizing species,

and its simplicity of the setup. Today, PLD is used to create depositions of a wide range of materials.

A simple diagram of a typically PLD process is shown in Figure 9: a vacuum chamber with a chamber window that has a holder for the substrate and a target material. To limit interaction of impurity gas molecules, a vacuum chamber is required. The substrate holder fixes the substrate in location and can alter the substrate in different ways such as heating or applying an electrical current. The target is used as source material to be deposited on the substrate. Finally, a pulse laser beam is directed at the target, resulting in the creation of an ablation plume towards the substrate which begins to form a film (Eason, 2007).

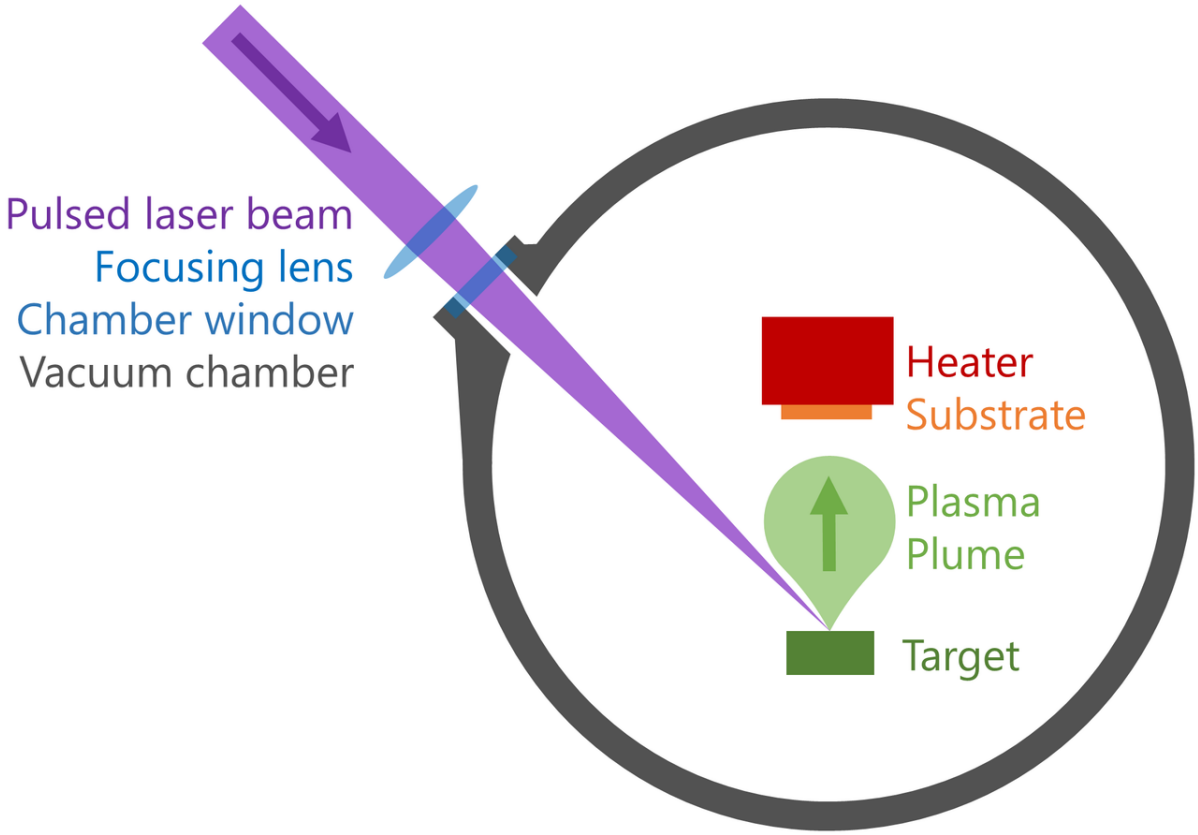

Figure 9: Image depicting the process of pulse laser deposition (Tedsanders, 2016)

The use of PLD to create ZnO thin films has been focused around p-type doping with copper (Q.A.Drmosh, 2012), gallium-phosphorus (W.S. Noh, 2016), and phosphorus-nitrogen (R. Mannam, 2015). The unique conditions of PLD allow for the formation of these nonequilibrium growth formations to remain stable after production. PLD does allow for the formation of high quality epitaxy grain growth but it does come with some limitations.

There are scalability issues with PLD. The use of a vacuum and the size of ablation plume limit the amount of substrate that can be used. Small sizes are good for creating hero cells for research, but are a limiting factor in production. The number of samples that can be created at a time is also limited by the size of the chamber and the time to create the vacuum. This results in a corresponding increase in costs with any increase in production.

Chemical Vapor Deposition

Chemical Vapor Deposition (CVD) is a very old processing technique dating back the late 1800's (Pierson, 1999). In its early years it was mostly used to produce high-purity refractory materials such as titanium and zirconium. After World War II, researchers began to take notice of the potential advantages that CVD offered and its use and popularity grew.

CVD is the deposition of a vapor onto a heated surface. It is part of a class of vapor-transfer processing techniques. With CVD, line of sight with the coating surface is not required, which allows for deposition on complex surfaces. It has a high deposition rate and can be used for thick coatings. It can allow for codeposition of elements and does not require a high vacuum.

Figure 10 shows a typical CVD process. The first step in CVD is thermal activation of the chemical precursors to form a vapor. This vapor is then transported through a heated chamber where the substrate is located. In this chamber, the desired gas phase reactions occur and the

reactants are deposited onto the substrate surface resulting in film formation. Volatile by-products are desorbed from the film and removed from the chamber through convection.

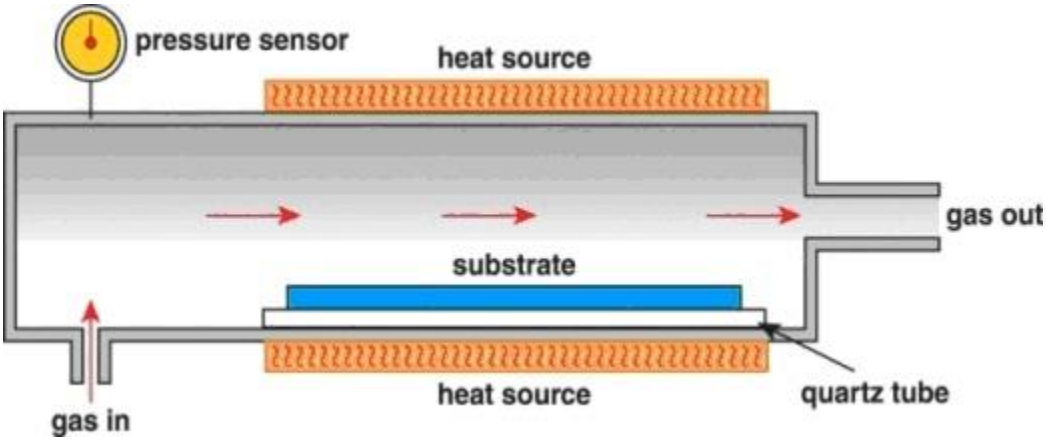

Figure 10: A typical CVD setup (Chemicals, 2013)

CVD typically requires high operating temperatures for the gas phase reactions to occur. This not only adds to the cost of processing but limits the types of substrates that the thin film can be grown on. The chemical precursors with high vapor pressures that are needed in CVD are typically toxic and hazardous to work with. Finally, the by-products from the gas phase reactions that do not remain on the thin films can also be toxic and even corrosion. Often it is required that these by-products be neutralized which adds to the cost of production.

Metal Organic Chemical Vapor Deposition

Throughout the years, several variations of CVD have been created to address some of the shortfalls. Metal organic CVD (MOCVD) is an example of this. The use of MOCVD began in the 1960's when it was used for the deposition of indium phosphide (Pierson, 1999). Those experiments demonstrated that epitaxial grown semiconductor materials could be produced at lower temperatures. MOCVD has expanded and is now heavily relied upon by the semiconductor and opto-electronic industries.

MOCVD has is the preferred processing method of various types of ZnO materials. It can allow for tight control over composition and deposition parameters. Production of samples as large as 30cm have been reported (B. Sang, 2003). However, MOCVD does have a limit to their scalability as samples can only be made in limited sized batches. Furthermore, the cost of neutralizing the volatile by-products adds to production costs. For large scale production, a processing technique should have low costs, little to no toxicity issues, and should scale easily.

A new route for processing has become popular called sol-gel (Znaidi, 2010). Sol-gel processing offers the potentials for a simplified, low cost, low energy, resource efficient processing route. Sol-gel allows the use of a solution or gel as a transition step between a liquid forming into a solid material. This is done through the conversion of liquid chemical solutions into an oxide network via hydrolysis and condensation reactions. This sol gel can then be applied onto a desired substrate though several different techniques. The samples then go through various drying and annealing stages to achieve the desired properties.

A sol is defined as a stable suspension of colloidal particles or nanoparticles in a liquid. These particles can range from amorphous to crystalline. They can be dense, porous, or even form polymer chains. A gel is a porous solid network surrounding and supporting a continuous liquid phase (Zayat, 2015). In typical sol-gel solutions, the formation of gels, or gelation, occurs when the sol particles form covalent bonds. The final structure of the gel network is dependent on the size and shape of these sol particles.

Sol-gel is also known as soft chemistry or solution chemistry. It is the process of taking a solid material, typically a metallic salt or alkoxide known and precursors, and transforming it into a sol or a gel. The transformation converts the metallic precursor into an oxide network

through hydrolysis and condensation reactions. This is process is typically done at either room temperature or up to no more than 100ºC, depending on the solvent used.

Figure 11 shows a typical sol-gel process for both thin films and powders (Znaidi, 2010). This process can be broken down into three main steps: preparation of the solution with a solvent, a precursor, and any additives that may be required. The solution is then applied to a substrate by several techniques with dip-coating (M. Ohyyama, 1997), spin coating (M.N. Kamalasanan, 1996) being the more commonly used.

The samples are then pre-heated at an elevated temperature to evaporate the solvent leaving behind a xerogel film or matrix. The process of applying the solution to the film/substrate and then dried is repeated until a desired film thickness is achieved. The sample is then post-heated, or annealed, to form the final crystal structure and remove any leftover organic material.

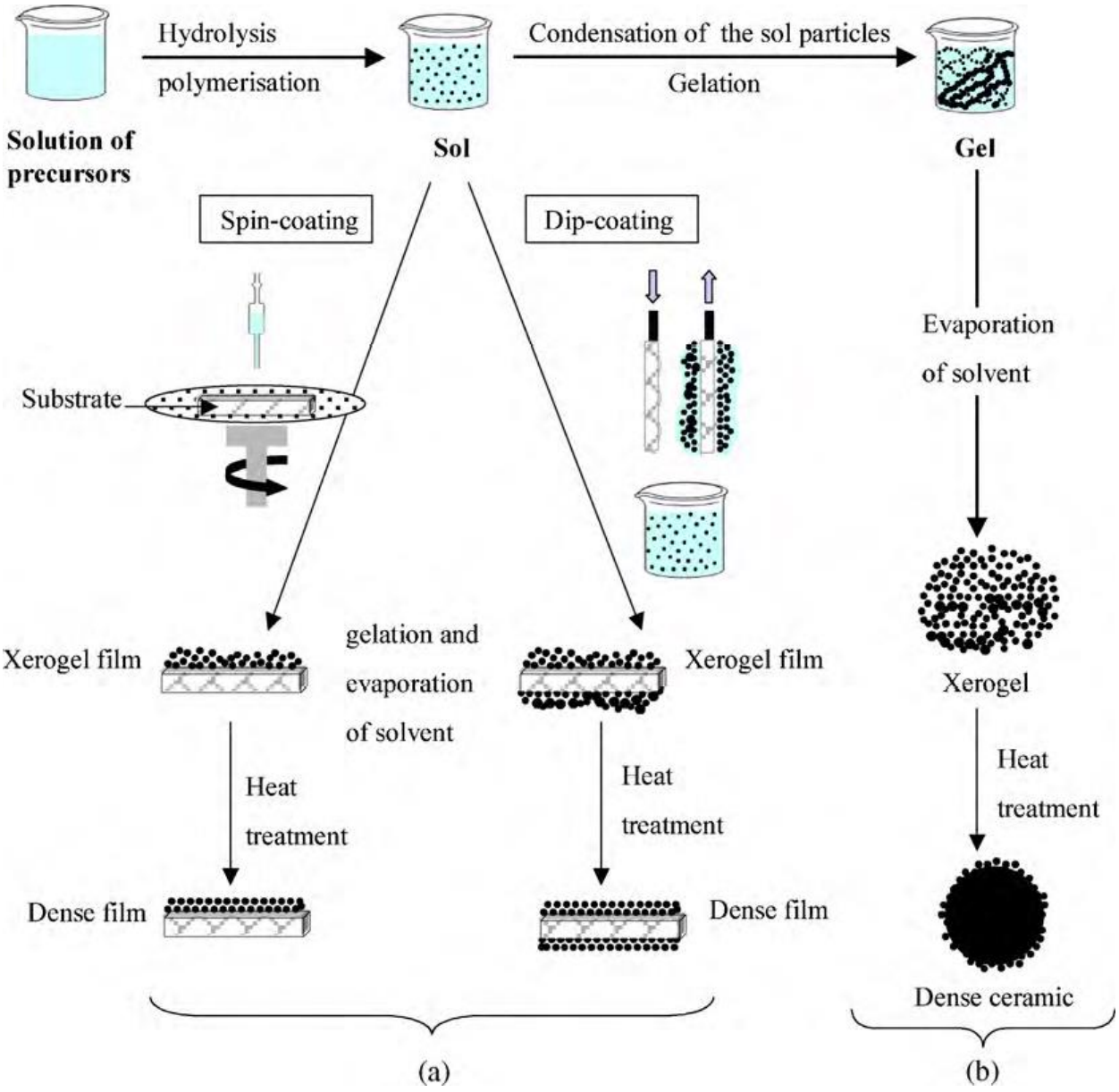

Figure 11: Image showing two synthesis routes using the sol-gel method. (a) demonstrates the formation of a dense film and (b) shows the formation of a powder or dense ceramic (Znaidi, 2010)

A sol-gel solution generally follows five main stages of formation which are hydrolysis, polymerization, condensation, nucleation, and growth (M. Hu, 2000) (Pierre, 1998). Two types of precursors can be used which will typically determine the solution used. Metal alkoxides are

generally used with organic solvents and metallic salts are used with aqueous solutions (J. Livage, 2001).

Sol-gel derived for ZnO however uses a hybrid of these two methods. Review of literature indicates that metallic salts are paired with organic solutions. By doing this, it is thought that two steps occur. First, there are in situ formation of either alkoxide or alkoxy complexes. Next these complexes go on to form into a solid metal oxide state via hydrolysis and polymerization.

When looking at possible precursors, there are several options available. Zinc alkoxides like ethoxide and propoxide seem like good options since alkoxides are typically used with alcoholic solutions. However, as Znaidi mentions (Znaidi, 2010), metal alkoxides are generally not desirable as they are, "sensitive to moisture, highly reactive and remain still rather expensive". Metallic salts, both organic and inorganic, are cheaper, readily available, and easier to work with relative to the metal alkoxides.

Inorganics zinc salts such as nitrates and chlorates are possible options for use; however, the anions in these species may be difficult to prevent from remaining in the final product. This leaves organic zinc salts like zinc acetate. The acetate groups that do remain in the gel will generally decompose during the annealing process of sample preparation. These combinations show why zinc acetate (ZnAC), specifically dihydrate, is the most commonly used precursor in ZnO thin film sol-gel (Znaidi, 2010).

Znaidi details that a high dielectric constant is need in a solvent for sol-gel chemistry. This will allow the solvent to properly dissolve the inorganic metallic salts that are commonly used. As these solvents will also be evaporated off the final sample, a low boiling point is

needed. Among organic solvents, alcohols are best equipped to handle this task. Ethanol (EtOH), methanol (MeOH), and 1 or 2 isopropanol (1 or 2-PrOH) are the most commonly used alcohols used as solvents for ZnO thin film sol-gels (Znaidi, 2010).

MeOH has one of the highest Dielectric constant, lowest boiling points, and lowest number of carbons. However, due to its high toxicity compared to the other alcohols, it should be avoided as it will not translate well to mass production. Between EtOH and 1 or 2 PrOH, EtOH has a higher dielectric constant, and lower boiling point. For these reasons EtOH will be used throughout this research.

The use of additive(s) can be employed to help facilitate shortcomings that may exist for certain precursor-solvent pairings. These additives can control the pH level, act as a chelating agent, or aid in dissolving the precursor in the solvent. The common pairing of ZnAC in alcohols like EtOH and PrOH typically require monoethanolamine (MEA) or diethanolamine (DEA) as an additive to help the organic salt fully dissolve.

Research has shown that solutions using DEA as an additive results in broad and poorly defined ZnO peaks while MEA solutions had sharp, well defined peaks. MEA, as a bidentate ligand, may act as chelating ligand on a single zinc atom or as a bridge between two zinc atoms. The combination of ZnAC, EtOH, and MEA is a common combination in other publications (Znaidi, 2010) and will be used exclusively throughout this research.

Characterization Methods

Characterization is the method of testing a sample and determining its properties. X-ray diffraction (XRD) is used to evaluate the crystal structure of a thin film. Scanning electron microscope (SEM) allow for indirect viewing of a surface at higher magnification than can be

obtain from a traditional microscope. Energy-dispersive X-ray spectroscopy (EDS or EDX) is used to analyze the elemental composition of both the surface as well a portion of the bulk material.

X-ray Diffraction

XRD has been around since 1912 and is one of the most common material characterization techniques used (Leng, Materials Characterization: Introduction to Microscopic and Spectroscopic Methods, 2013). Generally, there is very little sample prep require for use in XRD. It can be applied to a wide range of materials, even liquids. XRD is used to gather information about the nature of the crystals inside the samples. This can be used to determine the crystal structure, size, and sometimes even the chemical composition.

XRD characterization begins by shooting high-speed electrons and a metal source material. The energy from the colliding electrons in converted into X-ray radiation. Depending on the velocity of the electrons and the source material used, different wavelengths can be produced. For the Brucker model XRD machine used in this research, a 1.54Å wavelength X-ray beam is produced.

The X-ray beam will produce a series of parallel beams towards the target depicted in Figure 12. The dots represent atoms that are a distance, d_{hkl}, apart. The incident beams with interact with the atoms and be diffracted back out towards the detector. Bragg's law represents the difference between lengths of these two beams. The output of this equation is determined by the distances between these atoms.

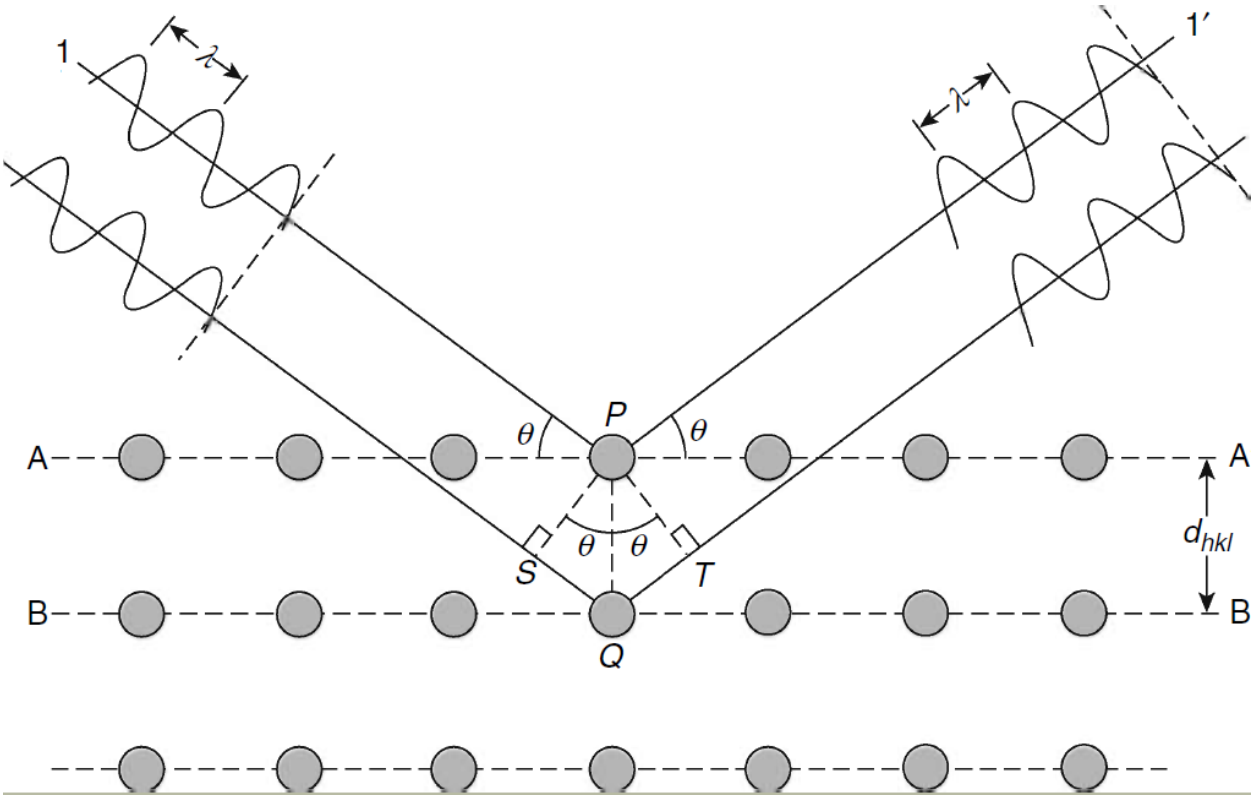

Figure 12: Image depicting an X-ray beam interacting with a sample (Leng, Materials Characterization: Introduction to Microscopic and Spectroscopic Methods, 2013) (Leng, Materials Characterization: Introduction to Microscopic and Spectroscopic Methods, 2013)

As the X-ray beams are being produced, the source and detector rotated about an axis to sweep for a range of angles on the samples. The source measures the "intensity" at different angle. This produces a graph like Figure 13. The two theta details the angle that the X-ray beam source and detector are at and the count is the measured "intensity".

The relative sharpness of the peaks details if the material is amorphous or crystalline in nature. The height, width, and location of the peaks provide information about the size of the crystals or grains for single crystal structures. This is done through the Scherrer equation, $T = K\Lambda/\mathrm{B}\cos\Theta$ where T is the size of the crystal, K is a constant, Λ is the wavelength of the X-ray beam, Θ is the Bragg angle. B is the full width of the peak at half the max intensity, known as full width half max (FWHM).

Finally, the location and in some cases the relative intensity of the peaks can tell us about the chemical composition of the material. All chemical compositions in a crystalline structure is going to have its own unique distances between atoms or crystal parameters; therefore, the XRD peaks produced can be thought of as finger prints for these chemical compositions. Using Figure 13 as an example, some analysis of this graph will tell us that these peaks are most likely the (100), (002), and (101) peaks of zinc oxide. Furthermore, the crystal size based of the (002) peaks is approximately 43nm.

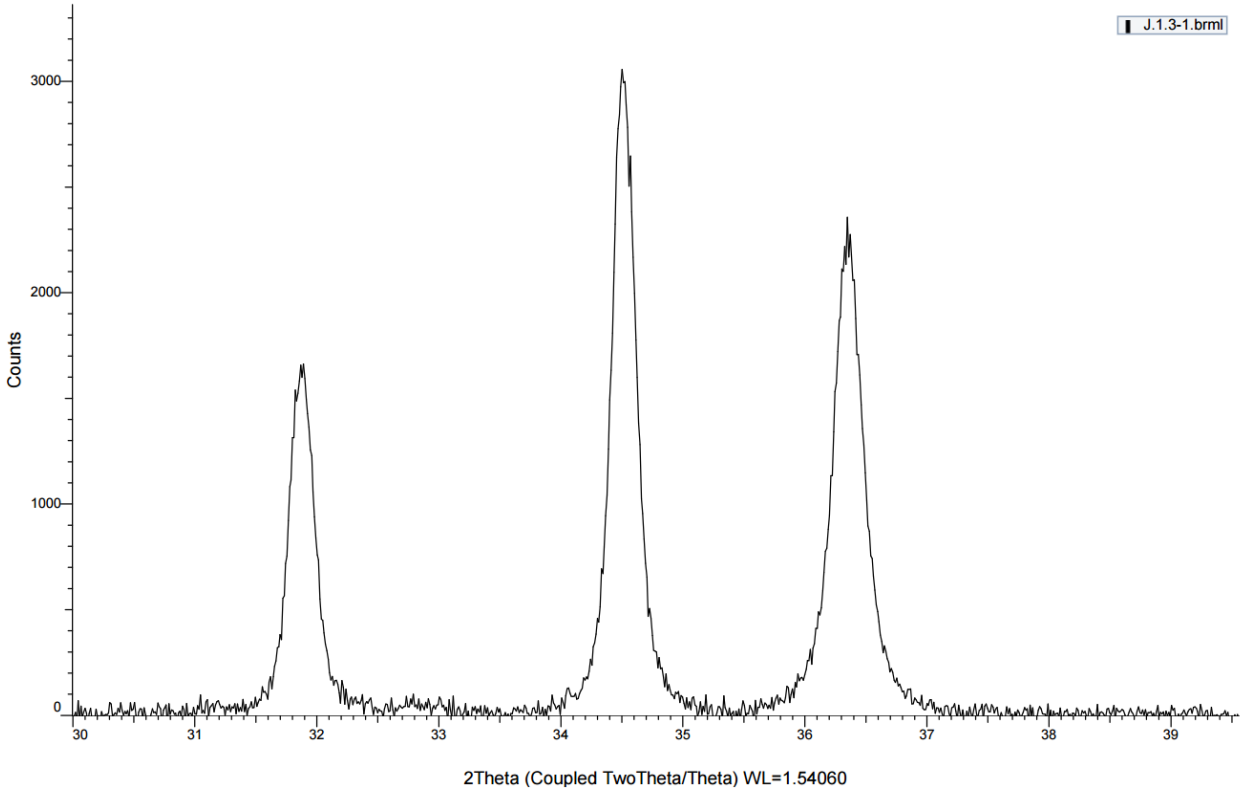

Figure 13: XRD result of a ZnO sample

Scanning Electron Microscope

Typical optical microscopes usually have a limit of around 1,000x to 2,000x magnification due to the nature in which they collect the image. Electron microscopes on the other hand can easily achieve 500,000x magnifications and the upper limit is only bound by the

equipment used and the skill of the operator. Unlike transmission electron microscopes (TEM) that forms an image from instantaneous illumination of a whole field, SEM relies on an electron beam that is focused on an area of a sample (Leng, Scanning Electron Microscopy, 2013).

The types of material and the condition of the samples are more important for SEM. Since SEM relies on the sample being bombarded with electrons, the sample must display some degree of conductivity. Materials like polymers and ceramics may require additional prep work of coating the sample with a thin (~2-5nm) layer of a conductive material such as iridium or a gold-palladium alloy. Furthermore, sample prep must be done in such a way to prevent things like fingerprints getting on the sample or sample holder as they may outgas under vacuum and damage the SEM equipment.

There is a wide variety of SEM equipment that serves a range of function. For this research as an example, two separate SEM machines were used. The first was a JEOL JSM-6460 LV with EDS. This has a tungsten filament and can achieve a vacuum of around 10^{-6} Torr. Images collected from this machine were typically between 1,000x to 7500x although it was predominately used for its EDS function.

For greater magnification to collect images used for surface analysis, a Hitachi S-4800 field emission (FE)-SEM was used. This uses a sharp point paired with a high voltage to produce the Electron beam. Images collected from this machine were typically between 25,00x and 200,000x magnification.

There is a large diversity of SEM equipment available but in generally they all follow the same principle. An electron beam is produced from various types of electrons guns and then is condensed into a beam or fine probe through a combination of electromagnetic lenses and

apertures. After the electron beam interacts with the sample individual electrons then go on to hit the detector.

There are two main detection types, backscattered electrons (BSEs) and secondary electrons (SEs) which detect electrons that were produced through elastic and inelastic scattering respectively shown in Figure 14. The detector then takes intensity of electrons and converts them into a digital image. Different materials will have a different reaction to the electron beam and this will show up as contrast in the image.

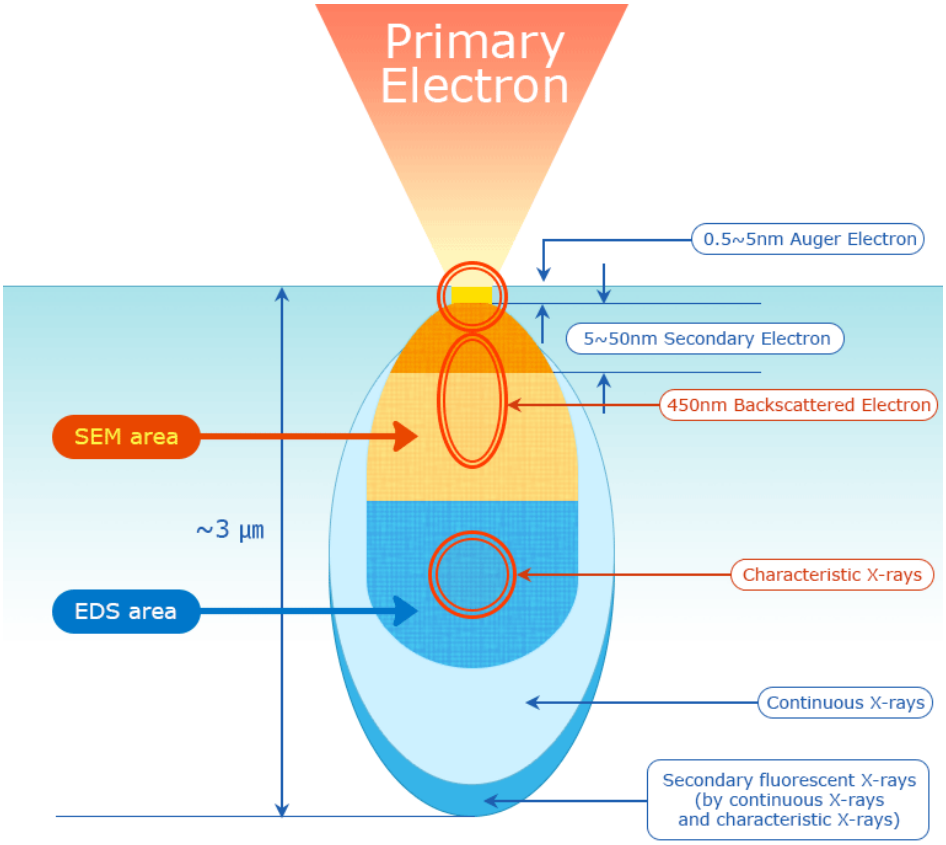

Figure 14: diagram showing the location of production of various electron "types" (SEM Technology, n.d.)

Energy Dispersion Spectrometry

EDS are commonly paired with SEM equipment as the same principle for sample analysis is used. Figure 14 details where both SEs and BSEs come from based on the depth into the sample. Up to and below this there is a level where characteristic X-rays can be produced. These characteristic X-rays are used to determine the various elements that are present within a sample.

These characteristic X-rays occur when the electrons from the electron beam strike the electrons of an inner orbital of an atom. The force of this strike will knock the electron out of the orbitals of the atom and becomes a "free" electron. The ionized atom then compensates for this by adjusting and electrons from higher orbitals begin to drop down to lower orbitals (Leng, X-ray Spectroscopy for Elemental Analysis, 2013).

Since there is an energy difference between orbitals, the electron must give off energy to move down. It releases this energy in several forms, including X-rays. This X-ray energy, which is the characteristic X-ray, is going to be unique to the orbital levels. Each atom will then have its own unique set of orbit energy differences. This allows the detection of the X-ray energy to be tracked back to an electron energy.

There are a couple of things to note about EDS. As Figure 14 demonstrates, EDS is not a surface analysis but instead a volume analysis. This is important for evaluating thin films as this depth is often larger than the thickness of the thin film. That means that elements from the substrate will be detected and must be accounted for.

Second, the peaks produced by EDS must be evaluated with care. Figure 15 is a typical EDS spectrum. In this example, it is a spectrum taken from a ZnO thin film on a glass substrate.

The x-axis represents the measured energy level and the y-axis is the count of that energy, of the amount of that element present. These peaks are fairly broad as opposed to being exactly at the energy level of the X-ray produced.

This results in in the peaks overlapping with each other. The middle of the peak can be used to determine an element; however, if the intensity of that peak is high and the peak is broad, a peak from a different element with a lower intensity could potentially be covered up by the other element. Conversely, a series of peaks from different elements can look like the collection of peaks from a single element. Although the autoID function of most EDS software is pretty good at filtering this out, the operator must use some intuition to determine if the elements chosen by the software is correct.

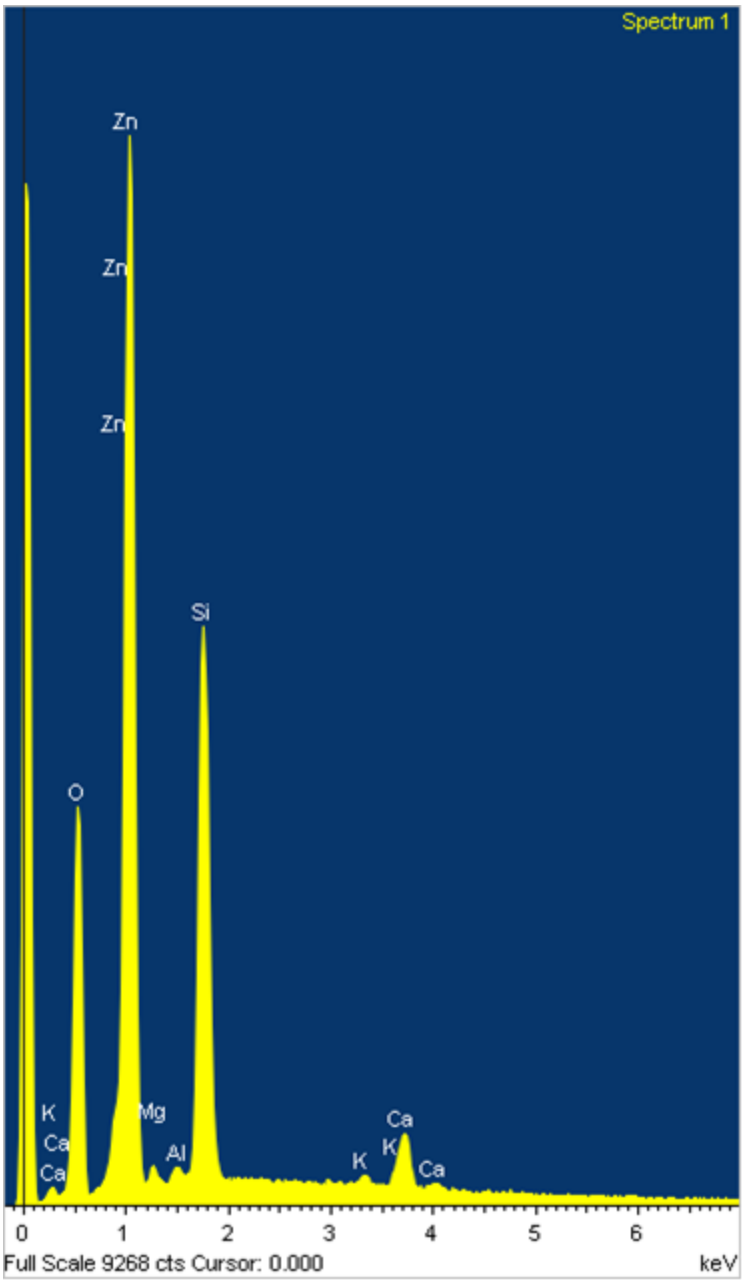

Figure 15: EDS spectrum of ZnO thin film on a glass substrate

Chapter 2: Effect of pre-heat (drying) temperature on the crystal structure of ZnO thin film

Objective

To study the effect of the drying temperature from 70ºC to 200ºC on the appearance and crystal structure of zinc oxide thin films prepared from an ethanol, zinc acetate, and monoethanolamine sol-gel solution.

Introduction

The pre-heat temperature, also known as the drying temperature, is commonly used in sol-gel processing between subsequent coats. This is done to evaporate the solvent and remove most of the organic compounds. Other studies have shown this parameter to influence the crystal structure and performance of the thin film for a variety of chemical systems.

The hexagonal wurtzite crystal structure is the most thermodynamically stable structure for zinc oxide (ZnO). This hexagonal close packed structure has an arrangement of zinc and oxygen atoms at tetrahedral site and has a space group of C^4_{6v} = p63mc. In wurtzite structures, lack inherent asymmetry, which results in anisotropic growth along the c-axis. This growth is perpendicular to the substrate surface and in ZnO is represented by the (002) peak. It was demonstrated by Li et al (Wen-Jun Li, May 1999) that the (002) orientation has the fastest growth velocity.

In reviewing a table prepared by Lamia Znaidi (Znaidi, 2010) showing that pre-heat temperatures ranging between 40ºC and 500ºC had been used previously (C. Shaoqaing, 2005) (S. Fujihara, 2001). Most these publications only used a single pre-heat temperature. In the rare case that the publication used any justification for that particular temperature, it was simply

basing its decision from a previous publication. A couple of studies did use two or more pre-heat temperatures (S. Fujihara, 2001) (M. Wang J. W., 2006) (G. Srinivasan, 2008).

Kim et al (Young-Sung Kim, 2005) studied the effect of the pre-heat temperature on a zinc acetate (ZnAcO), isopropanol, and monoethanolamine (MEA) chemical system. A range of pre-heat temperatures that were used: 200, 225, 250, 275, and 300ºC, for ten minutes. Following this, all samples were dried for one hour at 650ºC. XRD analysis showed that for this system, the highest (002) grain growth preference occurred at 275ºC.

Another publication by Shariffudin et al (S.S. Shariffudin, 2012) did analysis of the pre-heat temperature on a ZnAcO, 2-methoxyethanol, and MEA chemical system. The range of pre-heat temperatures that were used: 100, 150, 200, 250, and 300ºC, drying for ten minutes. The samples were then dried at 500ºC for one hour. XRD analysis showed that the highest intensity of the (002) was found in the sample dried at 200ºC. Above 250ºC the preference for (002) grain growth began to drop off.

Past research done on sol-gel derived ZnO thin films show a wide range of chemical systems used. However, publications never discuss why the exact solvent, precursor, and additive were used. For this research, a combination of ethanol (EtOH), ZnAcO, and MEA are used as solvent, organic metallic salt, and additive respectively. This arrangement is commonly used in research, as it offers the best solution for compatibility, cost, and toxicity level.

Although this particular chemical composition is commonly researched, there has not been a publication on the effect of the pre-heat temperature on the final thin film. For this research, a molar concentration of .75 and an r ratio (molar ratio between MEA and zinc) of 1, were chosen based on results from preliminary tests. Temperatures of 70, 120, 150, and 200ºC

were chosen as preheat temperatures. This low temperature range was chosen to study the viability that sol-gel processing could be is a low temperature, low cost processing technique.

Synthesis and processing

The solution was prepared by adding 1.646g of zinc acetate dihydrate (ZnAcO) and 10mL of 200 proof ethanol (EtOH) to an Erlenmeyer flask. Some of the ZnAcO dissolved immediately but much of it remained as undissolved salts. Next, 0.433g of monoethanolamine (MEA) was added gravimetrically and the remaining ZnAcO fully dissolved to produce a clear solution. Then, the entire solution was placed on a hot plate set to 60°C and stirred at 250 rpm for one hour. Finally, the solution was covered with parafilm and stored in a dry, dark place and allowed to age at room temperature for 24 hours.

Glass microslides 3" x 1" were prepared by first cutting and sectioning them into three, 1" x 1" slides. They were then marked for identification on the reverse side of the surface to be coated. This was done so that the etching did not disturb the application of the solution. Slides were then hand washed with dish soap and then placed in a dilute nitric acid bath for ten minutes. They were then rinsed off with deionized water (DI) and ethanol, and then dried in a 100°C oven for ten minutes.

The first sets of samples were then prepared by taking the cleaned glass substrates out of the oven and placed on the spin coater. As the sample was rotating, 3-4 drops of the solution were applied to the substrate. The sample was spun at 3000 rpm for 30 seconds and then they were place in a 70°C oven for approximately ten minutes to dry. This process was then repeated three additional times for a total of four coats. Finally, the samples were placed in a 500°C furnace to be annealed for one hour. This entire procedure was repeated for each set of samples at additional drying temperatures of 120°C, 150°C and 200°C.

Characterization

Visual Observations

Visual analysis of the prepared samples was performed with a stereoscope for lower magnification, in order to observe appearance and surface features. For these images, a black background was used for contrast. A comparison of the images gathered from each set is shown in Figure 16.

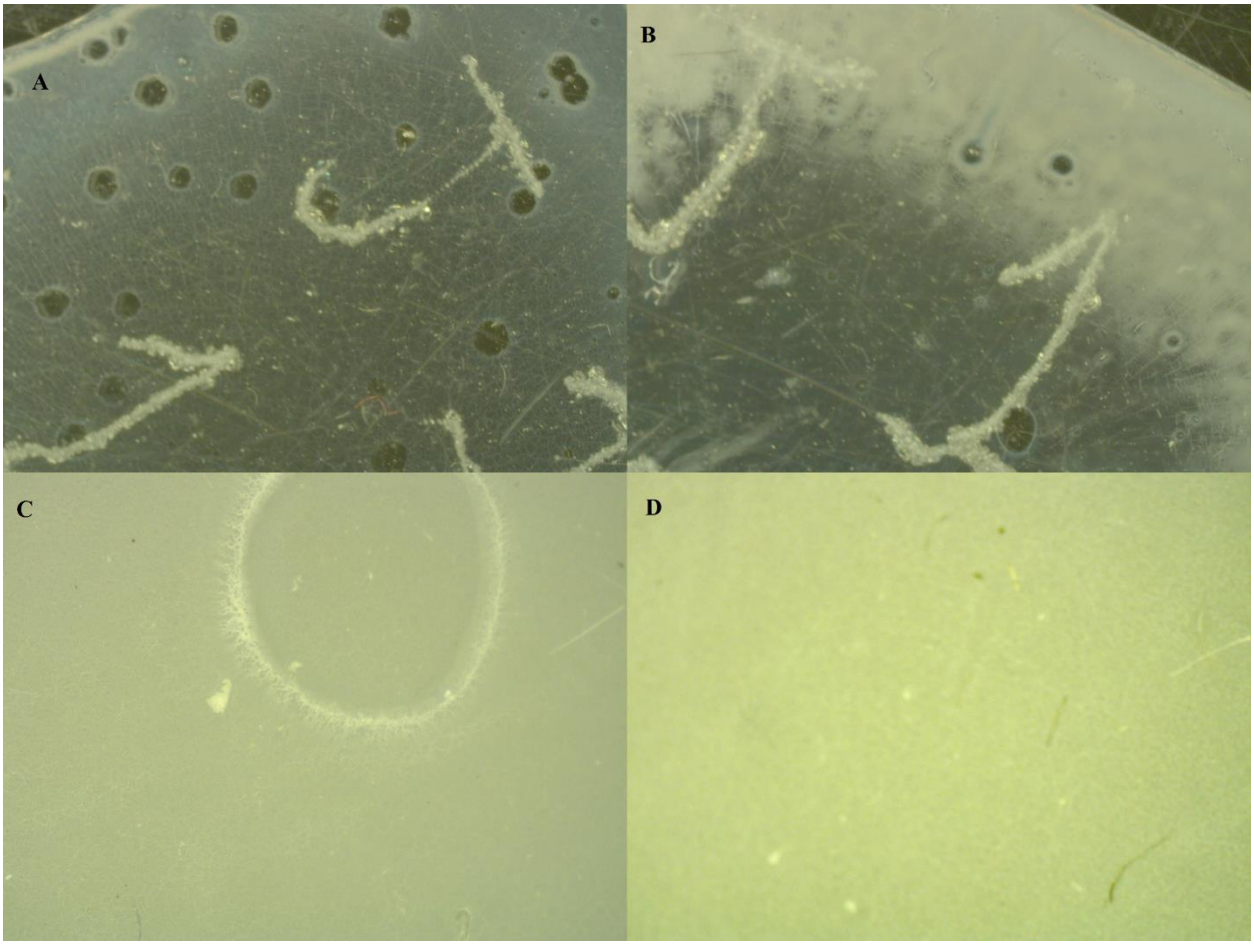

Figure 16: comparison of images taken from a stereo microscope of samples dried at 70°C (A), 120°C (B), 150°C (C), and 200°C (D)

For samples A and B, the transparency of the film is high enough that the etching of the slides and the black background is still apparent. There are also observed circles or voids in the ZnO thin film of these two samples. Beginning with sample B, an opaque edge is observed

encroaching in towards the center of the sample. In C, the opacity has covered the entire sample. In sample D, the black background can no longer be distinguished.

XRD Analysis

Structural analysis of the samples was carried out by x-ray diffraction. Before the samples were tested, a corundum standard was run and the accuracy of the machine was verified. The parameters of the machine were 40 kV and 40mA with a CuKa1 source with a wave length of 1.54nm. The tests were run at 40 mA and kV between 30° and 40° two-theta. This narrow and small angle range was chosen to analyze the three major peaks, (100), (002), (101) for (ZnO).

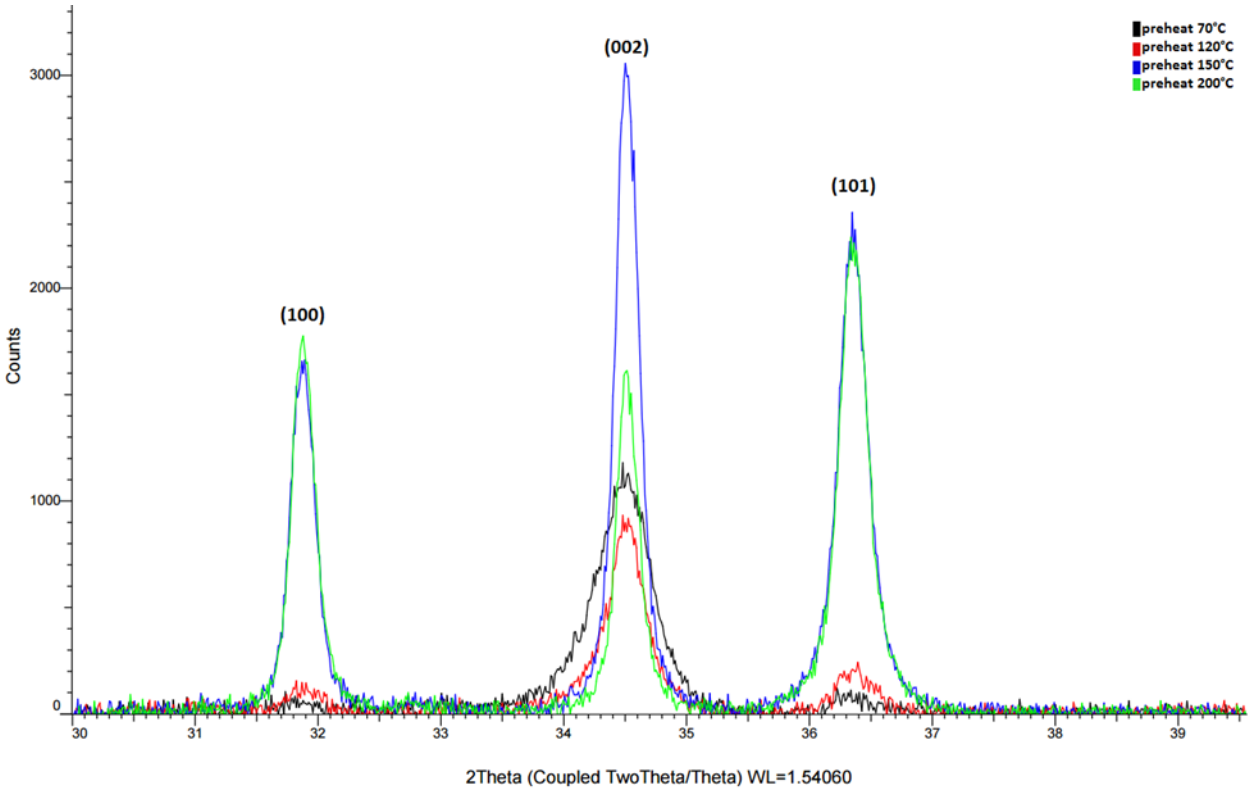

Figure 17: XRD graph comparing samples dried at 70, 120, 150, and 200C

Figure 17 displays the XRD graphs for each sample set on top of one another. Samples A and B show (002) grain growth preference with poor definition. In sample C, the definition and intensity of the (002) increases; however, there is no longer a preference for the (002) peak as the

intensity of the (100) and (101) peaks are also increased. The intensities of these peaks at (100) and (101) remain the same for sample D; on the other hand, the intensity of (002) preference is no longer present.

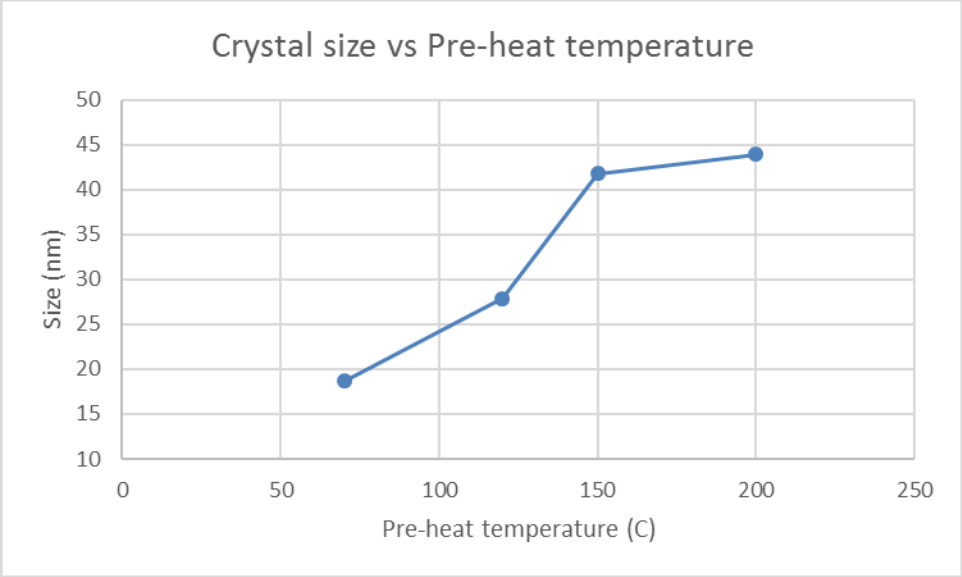

Figure 18: graph showing the relationship between the pre-heat temperature and the crystal size of the (002) peak

XRD analysis was also done to gather the crystal size of the thin films based on the (002) peak. Figure 18 shows that as the drying temperature increased from 70°C to 150°C the crystal size also increased. Between 150°C and 200°C there was a small, less than 2 nm, increase in crystal size. This would suggest that there is an upper limit to the grain size that can be achieved by adjusting the pre-heat temperature.

Summary

XRD analysis and stereoscope images show that as the drying temperature increases, grain size also increases but transparency and (002) grain growth preference decrease. This is attributed to a higher evaporation rate of the solvent which decreases the mobility of the particles and structure of the thin film.

Discussion

The images collected via stereo microscope show that the samples are less transparent, even opaque, as the drying temperature increased. Although these features were less likely to form at lower temperatures, this was not entirely reproducible. This would indicate that although the drying temperature may affect the apparent transparency of the films, there are other, unknown variables that need to be accounted for.

The appearance of the circles or voids is a bit of a mystery. It does appear that at the center of these circles there are tiny specs. These specs may be the formation of large particle zincite. Perhaps when these larger particulates form, they soak up the material around them and continue to grow. A lower drying temperature would result in a lower evaporation rate allowing for a higher degree of solution mobility. This would explain the higher concentration of spots on the lower temperature prepared films.

The XRD graphs show that as the drying temperature is increased, there is a lower preference for (002) grain growth. This is in line with the publications discussed earlier that studied the effect of pre-heat temperature on the crystal structure. There appears to be a critical temperature in which (002) grain growth is no longer preferred. This critical temperature appears to be lower than for other chemical systems as the boiling point of EtOH and MEA is lower.

Another direct observation from the comparative XRD graph shows that for samples A and B there is a more amorphous structure and for samples C and D, a shift to a crystalline structure is seen. This can be explained by the different drying temperatures affecting the drying rate of the solution. The lower drying rate allows the liquid solution to remain on the substrate. The solvent allowed for more time and mobility of the xerogel, allowing it to relax and become amorphous before crystallization begins.

It is shown that the grain size increase with an increase in the drying temperature despite all samples being annealed under similar conditions. As discussed above, a lower drying temperature and subsequent less evaporation, results in a film that has more mobility and time to allow for relaxation of the xerogel. This would indicate that at higher temperatures, a more crystalline structure is used as a seed for crystal growth. This would result in the formation of larger crystal cells.

Future work

This research demonstrates that a low temperature, low cost ZnO thin film can be obtained through an EtOH, ZnAcO, and MEA solution. It also shows that different drying temperatures will result in films with very different appearance and crystal structure. Different crystal structures will be more appealing to different research topics.

The drying temperature can be changed and optimized for a range of desired properties. There are two topics that come to mind for future research. First, the upper range of the drying temperature can be expanded. Although a lower temperature is desired, higher temperatures may be required to obtain specific properties. A smaller incremental change between temperatures should also be studied to allow for further optimization.

References

C. Shaoqaing, Z. J. (2005). Nanocrystalline ZnO thin films on porous silicon/silicon substrates obtained by sol–gel technique. Applied Surface Science volume 241, 384-391.

G. Srinivasan, N. G. (2008). Influence of post-deposition annealing on the structural and optical properties of ZnO thin films prepared by sol–gel and spin-coating method. Superlatticies and Microstructures volume 43, 112-119.

M. Wang, J. W. (2006). Effect of preheating and annealing temperatures on quality characteristics of ZnO thin film prepared by sol–gel method. Materials Chemistry and Physics volume 97, 219-225.

S. Fujihara, C. S. (2001). Crystallization behavior and origin of c-axis orientation in sol–gel-derived ZnO:Li thin films on glass substrates. Applied Surface Science volume 180, 341-350.

S.S. Shariffudin, M. H. (2012). Influence of drying temperature on the Structural, Optical, and Electrical properties of Layer-by-Layer ZnO nanoparticles seeded Catalyst. Journal of Nanomaterials volume 2012, Article ID 359103, 7.

Wen-Jun Li, E.-W. S.-Z.-W. (May 1999). Growth mechanism and growth habit of oxide crystals. Journal of Crystal Growth volume 203 issue 1-2, 186-196.

Young-Sung Kim, W.-P. T.-J. (2005). Effect of preheating temperature on structural and optical properties of ZnO thin films by sol-gel process. thin solid films 491, 153-160.

Znaidi, L. (2010). Sol-gel deposited ZnO thin films: A review. Material Science and Engineering B.

Chapter 3: Silver Doped Zinc Oxide Solutions

Objective

Attempt to make a silver doped zinc oxide thin film through sol-gel technique. Solution was prepared with ethanol, zinc acetate, monoethanolamine, and silver nitrate.

Introduction

Literature review done by Minami (Minami, 2005) shows that over the last several years the conductivity of undoped zinc oxide (ZnO) has begun to plateau. This would suggest that undoped ZnO is reaching its potential for conductivity. Extrinsic doping will allow for improvement and specialization of a wide range of properties including electrical.

Undoped ZnO is a native n-type semiconductor. This is the result of native defects that occur in ZnO (C. H. Park, 2002) (S. B. Zhang, 2001) (Yanli Liu, 2013). Hole killer defects such as zinc interstitial and oxygen vacancies have low formation energies and occur more readily. Electron killer defects such as oxygen interstitial and zinc vacancies have higher formation energy and occur less frequently.

Popular ZnO doping elements are group IIIA and group VII elements (Yanli Liu, 2013). First principle calculations by Yim et al (K. Yim, 2017) show the formation energies of a wide range of elements. These calculations show that group IIIA elements have low formation energy for zinc substitution and group VII element have low formation energies for oxygen substitution. Both of these situations result in hole killer defects.

To form a p-type material, group I and group VA elements are often considered. Yim et al's calculations show that group I element at interstitial sites form more readily that at zinc substitution sites. Analysis of group VA elements shows that nitrogen phosphorus and arsenic

would rather form substitutionally with zinc than oxygen. Park et al also performed first principle calculations on these elements with a more detailed analysis. They found that doping with these elements leads to an increase of compensating interstitial formation. This makes it more difficult to make a p-type doped ZnO with these elements.

Park et al's analysis ignores another potential group for p-type doped ZnO. This is the group IB elements copper, silver, and gold. First principle calculations on doping ZnO with group IB elements was carried out by Yan et al (Yanfa Yan, 2006) and are replicated by Kim's recent calculations. The results show that under oxygen rich conditions all the group IB elements have low formation energies at zinc substitution sites. These works also show that the hole killer defects are suppressed.

Some experimental work has been done on sol-gel derived ZnO thin films doped with group IB elements (R.K. Gupta, 2010) (S.M. Ali, 2015) (S. Khosravi-Gandomani, 2013); however, there was one publication by Touam et al (T. Touam, 2015) that outshone the others and was utilized as a baseline to preform several preliminary tests. These tests demonstrated the difficulty of working with silver in solution. It was also discovered that care must be taken to limit the solutions exposure to light as this would result in photoactivating of the silver state.

The goal of this research was to test the viability of doping zinc oxide with a range of 1, 2, 3, and 4% silver concentration. Silver nitrate was chosen for the metallic salt as this was the salt used to replicate the results of Touam et al. When preparing the solution, it was determined that a molarity of .75 would still be acceptable. It was found that the molar ratio between the metal salts and the MEA should be increased to 1.2 otherwise the salts would not fully dissolve.

Synthesis and processing

Four solutions, 1, 2, 3, 4, were prepared with various dopant concentration of silver. Solutions were prepared by adding the metallic salts, zinc acetate (ZnAcO) and silver nitrate ($AgNO_3$) to 99.5% pure ethanol (EtOH). To fix the molarity to .75, the EtOH was held constant and as the $AgNO_3$ was increased, the ZnAcO was decreased. MEA was added dropwise to fully dissolve the metallic salts. The actual values of ZnAcO and $AgNO_3$ for solution 1, 2, 3, and 4 are detailed by Table 1.

Table 1: Chemical composition for solution 1, 2, ,3 and 4

Solution	g AgNO3	mol AgNo3	g ZnOAc	mol Zn	at% Ag:Zn	[Ag:ZnO] M
1	6.540E-03	3.850E-05	8.162E-01	3.718E-03	0.010	0.751
2	1.308E-02	7.700E-05	8.086E-01	3.684E-03	0.021	0.752
3	1.962E-02	1.155E-04	8.006E-01	3.647E-03	0.032	0.753
4	2.616E-02	1.540E-04	7.926E-01	3.611E-03	0.043	0.753

The solutions were prepared under limited ambient light and the Erlenmeyer flasks were covered with aluminum foil to limit the exposure of $AgNO_3$ to light. All solutions were set on a magnetic heat plate set to 60°C and stirred at 250 RPM for one hour. The appearance of the solution was clear and homogenous without precipitates. The samples were then covered with parafilm and stored in a dry, dark place and allowed to age at room temperature for 24-48 hours.

Glass microslides 3" x 1" were prepared by first cutting and sectioning them into three, 1" x 1" slides. They were then marked for identification on the reverse side of the surface to be coated. This was done so that the etching did not disturb the application of the solution. Slides were then hand washed with dish soap and then placed in a dilute nitric acid bath for ten minutes. They were then rinsed off with deionized water (DI) and ethanol, and then dried in a 100°C oven for ten minutes. The 4 solutions would then be used to make 4 sets with 3 duplicates.

The first sets of samples were then prepared by taking the cleaned glass substrates out of the oven and placed on the spin coater. As the sample was rotating, 3-4 drops of the solution were applied to the substrate. The sample was spun at 3000 rpm for 30 seconds and then they were place in a 100°C oven for approx. ten minutes to dry. This process was then repeated three additional times for a total of four coats. Finally, the samples were placed in a 500°C furnace to be annealed for one hour. This entire procedure was repeated for the three other solutions.

Characterization

XRD Analysis

Structural analysis of the samples was carried out by x-ray diffraction. Before the samples were tested, a corundum standard was run and the accuracy of the machine was verified. The parameters of the machine were 40 kV and 40mA with a CuKa1 source with a wave length of 1.54nm. The experiment tested the range of 30° to 80° two-theta. The reason for the larger spectral range was to see if any metallic silver peaks appeared.

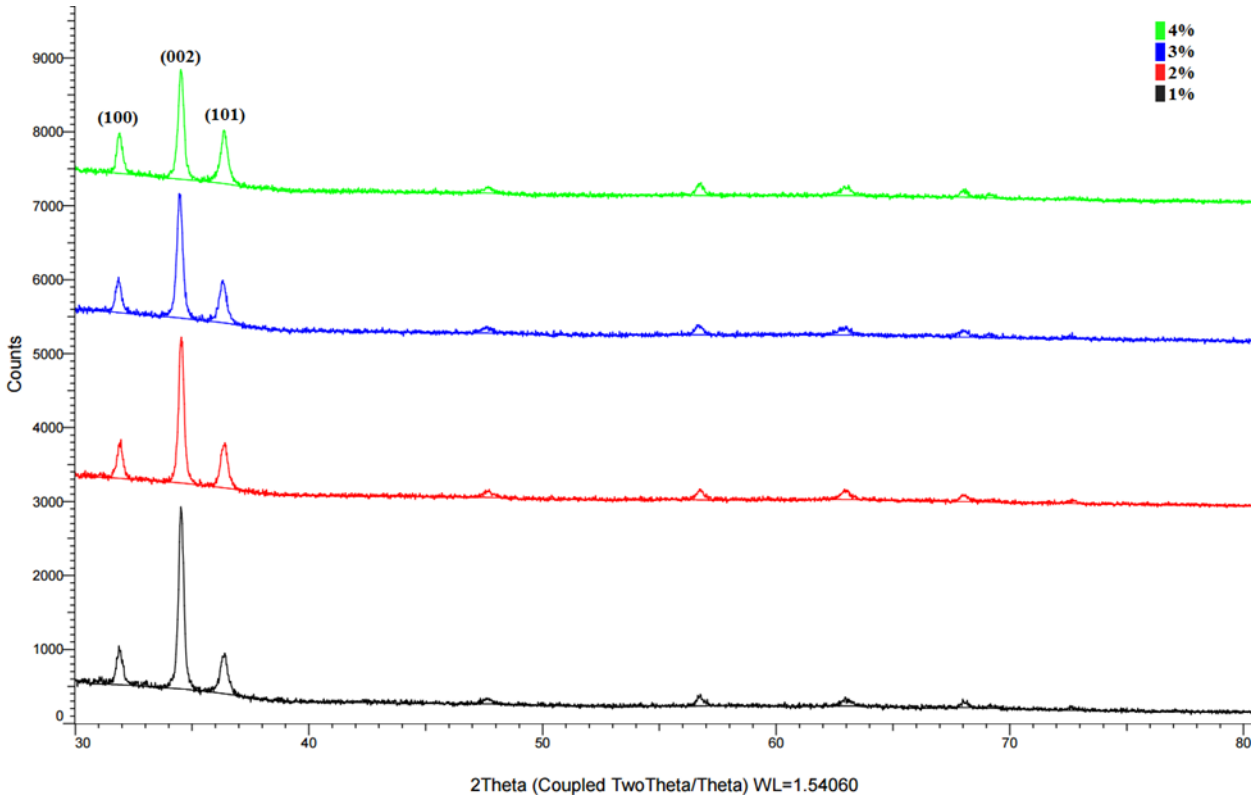

Figure 19: XRD analysis of the samples made from the 4 different solutions

Figure 19 compares the XRD results of samples taken from each concentration. The measured crystal size of the (002) peaks for the 1, 2, 3, and 4% samples were 37.7, 36.8, 33, and 34.7 nm respectively. The graph shows that the intensities of the (100) and (101) peaks maintain a similar intensity. However, as the silver concentration in the solution increases, the intensity of the (002) decreases resulting in a lower (002) grain preference.

EDS

One sample from each set was chosen to be analyzed in an energy-dispersive X-ray spectrometer machine. The samples had a working distance of 13mm under an electron beam that was set to 15kV. The spot size was set to 47 to achieve a dead time of around 19-20%. The spectra process was allowed to collect the data for two minutes. Each sample had spectra taken at three sites of interest to ensure the homogeneousness of the thin film.

It is important to note that when analyzing the EDS data, silver had to be manual checked for after each test. This signifies that the software's auto identification function did not feel there was sufficient data to include the silver analysis. This is important since the silver peaks do not overlap with the peaks of the other elements that were observed. That means that the silver peaks would be measured based on background noise and not "hidden" behind another element.

1%		2%		3%		4%	
Element	Atomic %	Element	Atomic %	Element	Atomic %	Element	Atomic %
Zn	35.69	Zn	37.61	Zn	31.27	Zn	36.86
Ag	0.00	Ag	0.05	Ag	0.09	Ag	0.39

Table 2: Table comparing the atomic ratio between zinc and silver in the 4 separate solutions

Table 2 provides a comparative analysis of the measured atomic weights for zinc and silver for the four different solutions. The table only presents the data for zinc and silver atomic percentage, leaving out the oxygen as well as elements found in the glass substrate. This narrow view is due to the relative ratio of silver to zinc being of primary interest to this paper.

The large and unpredictable change in the atomic percent of zinc is most likely due the changes in thickness of the ZnO thin film at the locations taken. Although the silver concentration in the different solutions maybe an explanation for change of thickness; this test is not able to confirm this hypothesis. The table shows that the atomic percent of silver increases with a higher percent of silver in the solution; however, the ratio between these two are much less than expected amount of silver.

Summary

XRD analysis showed that solutions with a higher amount of silver concentration resulted in a lower preference for (002) grain growth. However, XRD and EDS analysis could not directly confirm the presence of silver in the zinc oxide film.

Discussion

Despite silver needing to be manually analyzed for, the fact that the ratio of silver to zinc increases with an increase of silver in the corresponding solutions indicates that there is silver present in the ZnO thin film, albeit less than expected. The XRD results show that there is a change in the intensity of the (002) peak between the solutions. The lower intensity in the solution with higher silver content may suggest that the inclusion of silver is inhibiting the preferential growth of the (002) grains.

Although it is reasonable to say that there is silver in the ZnO thin films, it is a bit of a mystery why the content is so low. Some preliminary tests done on copper doped solutions turned up the same results. The inclusion of the new metallic species made changes to the ZnO structure, but could not be definitively found directly through either XRD or EDS results. It is also not entirely clear what would happen to the metal if it was not on the film or in a powder.

Future work

Future research in sol-gel derived doped ZnO must begin with the chemistry. The chemistry is well understood for undoped sol-gel solution. However, the effect of an additional metallic salt has not been studied. Further research is needed to understand what is happening inside the solution to verify that the doping element is in fact ending up inside the ZnO crystal structure and not just grouping up to form nano particles or particulates.

Silver was chosen because it was suggested that it would be the best candidate for making a p-type doped ZnO thin film. Copper also has potential with the added benefit that it is cheaper and more conductive than silver. Preliminary solutions were attempted but no copper doped ZnO thin films were ever created. If the solution chemistry can be figured out for silver as a dopant, copper should also be considered a candidate for testing as well.

Finally, if doping with type 1B elements in ZnO is shown to be possible, a comparative study on doping concentrations is necessary. There is certainly an optimal amount of dopant material that provides the best properties.

References

C. H. Park, S. B.-H. (2002). Origin of p-type doping difficulty in ZnO: The impurity perspective. Physical Review B.

K. Yim, J. L. (2017). Property database for single-element doping in ZnO obtained by automated first-principle calculations. Nature scientific reports 7.

Minami, T. (2005). Transparent conducting oxide semiconductors for a transparent electrodes. Institute of physics publishing.

S. B. Zhang, S. -H. (2001). Intrinsic n-type versus p-type doping asymmetry and defect physics of ZnO. Physics review b, volume 63.

T. Touam, F. B. (2015). Effect of silver doping on the structural, morphological, optical, and electrical properties of sol-gel deposited nanostructured ZnO thin films. Optik 126, 5548-5552.

Yanfa Yan, M. M.-J.-H. (2006). Doping of ZnO by hroup-1B elements. Applied physics letters.

Yanli Liu, Y. L. (2013). ZnO-Based Transparent Conductive Thin Films: Doping, Performance, and Processing. Hindawi Publishing Corporation, Journal of Nanomaterials.

Chapter 4: Effect of Annealing Temperature on Crystal Structure and Surface Properties

Objective

To study the effect of the annealing temperature from 300°C to 500°C on the surface feature and crystal structure of zinc oxide thin films prepared from an ethanol, zinc acetate, and monoethanolamine sol-gel solution.

Introduction

The post-heat temperature is more commonly known as the annealing temperature. It is typically the last stage of processing for sol-gel derived zinc oxide (ZnO) thin films. The main purpose of annealing is to provide the driving force for diffusion and crystallization of the thin film. Secondary purpose may include further decomposition of any remaining organic material from the original solution.

It is without question that the annealing temperature will have an effect on the crystal structure of the ZnO thin film. Studying the exact effect has been tested over a wide range of chemical systems (Znaidi, 2010) (D. Bao, 1998) (A.E. Jimenez-Gonzalez, 1998) (M. Wang E. K., 2006) (M.P. Bole, 2009) (L.Y. Lin, 2009) (M. Wang J. W., 2006) (H.Y. Bae, 1999) (Y. Caglar, 2009) (M.W. Zhu, 2008) (B.K. Choi, 2006) (G.T. Delgado, 2009). It has even been studied on the chemical system of ethanol (EtOH), zinc acetate (ZnAcO) (J. Wang, 2007), and monoethanolamine (MEA) that is used throughout this research.

There are some gaps that appear in the studies done on the annealing temperature however. The pre-heat temperature is never constant and the effect it has on the crystal structure is never accounted for in these publications. As discussed in a separate study, the pre heat temperature affects the evaporation rate of the solution. This in turn, affects the time of mobility

of the xerogel which will affect the crystal seeds for grain growth. The changes in the crystal seeds could potentially have different effects for different annealing temperatures.

Although the crystal structure has been evaluated, the main purpose of this study was the surface features of the film. ZnO thin films produced through various preliminary works have proven the difficultly to measure the electrical properties. For reference, the resistance of a typical commercially bought ITO glass slide can be measured with a multimeter. Although this simple test is not a high reliability test, it does show continuity of the thin film in the X-Y plane.

Since the ZnO thin films produced through preliminary work failed this simple multimeter test, it was thought that the thin films produced lacked continuity. It was theorized that the thermal shock experienced by the thin film after annealing contributed to cracks or discontinuity of the film. The first step in determining the contributions to film continuity was to adjust the annealing temperature.

The samples prepared in preliminary work were simply removed from the furnace after one hour of annealing. This air quenching results in a high degree of thermal shock and has even fractured the glass substrates. A lower annealing temperature should result in a lower degree of undercooling, thus lower thermal shock. High resolution scanning electron microscope (HRSEM) would allow for analysis of surface features of the thin films.

Synthesis and processing

The solution was prepared by adding 1.646g of zinc acetate dihydrate (ZnAcO) and 10mL of 200 proof ethanol (EtOH) to an Erlenmeyer flask. Some of the ZnAcO dissolved immediately but much of it remained as undissolved salts. Next, 0.433g of monoethanolamine (MEA) was added gravimetrically and the remaining ZnAcO fully dissolved to produce a clear

solution. Then, the entire solution was placed on a hot plate set to 60°C and stirred at 250 rpm for one hour. Finally, the solution was covered with parafilm and stored in a dry, dark place and allowed to age at room temperature for 24 hours.

For this research, ITO coated slides were used in place of standard glass slides. The ITO coated glass microslides 3" x 1" were prepared by first cutting and sectioning them into three, 1" x 1" slides. They were then marked for identification on the reverse side of the surface to be coated. This was done so that the etching did not disturb the application of the solution. Slides were then hand washed with dish soap and then placed in a dilute nitric acid bath for ten minutes. They were then rinsed off with deionized water (DI) and ethanol, and then dried in a 100°C oven for ten minutes.

Samples were then prepared by taking the cleaned glass substrates out of the oven and placed on the spin coater. Scotch tape was used to cover approximately half of the samples. As the sample was rotating, 3-4 drops of the solution were applied to the substrate. The sample was spun at 3000 rpm for 30 seconds. The scotch tape was removed from the sample before it was placed in a 100°C oven. After the samples were allowed to dry for about seven minutes, a new piece of scotch tape was replaced where the old piece was. The tape was replaced due to at the elevated temperature of the oven; a portion of the adhesive from the tape would remain on the sample as an impurity.

The final three sets of samples were made by repeating the above process four times in order to create multiple coats. The first set was placed in an oven at 300°C, the second at 400°C and the last set at 500°C. The samples were annealed at their respective temperatures for one hour and removed from the furnace and effectively air quenched.

Characterization

XRD

Structural analysis of the samples was carried out by x-ray diffraction. Before the samples were tested, a corundum standard was run and the accuracy of the machine was verified. The parameters of the machine were 40 kV and 40mA with a CuKa1 source with a wave length of 1.54nm. The tests were run at 40 mA and kV between 30° and 40° two-theta. This narrow and small angle range was chosen to analyze the three major peaks, (100), (002), (101) for (ZnO). A comparative XRD graph is shown in Figure 20, below.

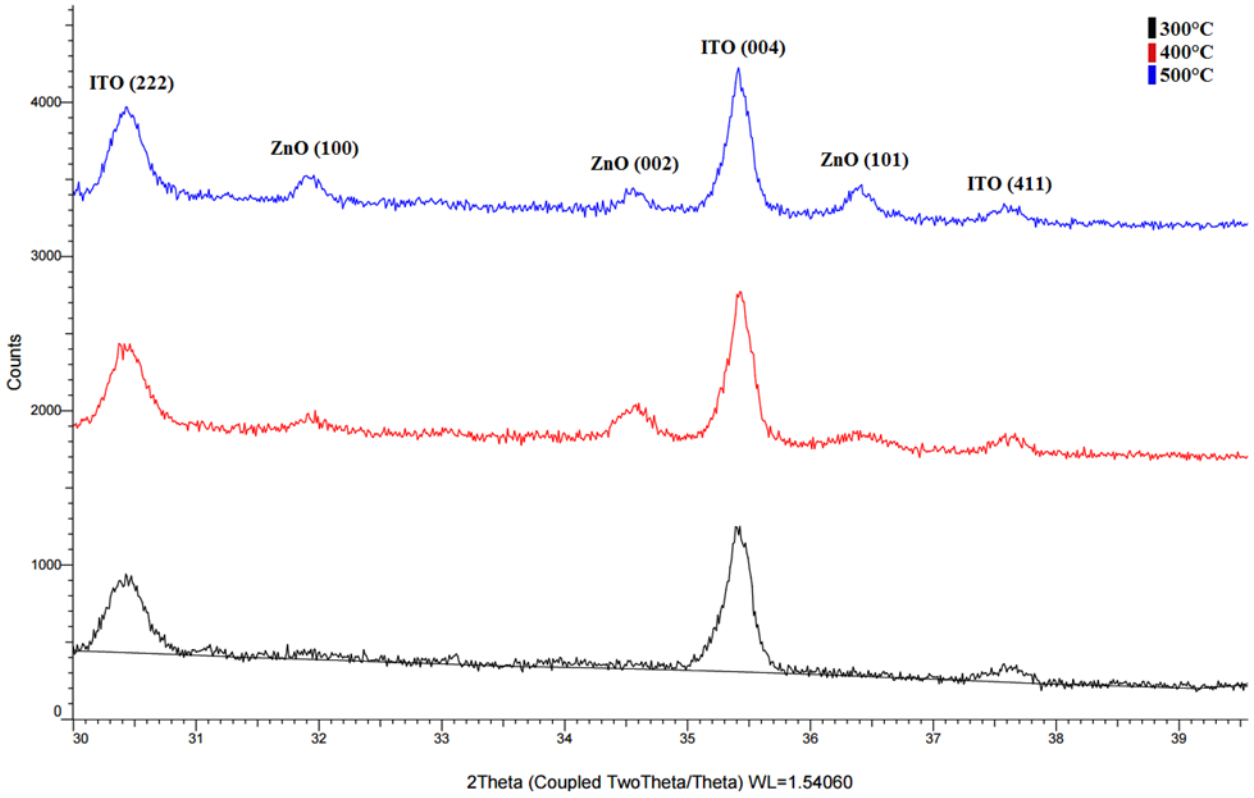

Figure 20: Graph comparing the ITO and ZnO peaks of samples annealed at 300, 400, and 500°C

The ITO peaks have been labeled to distinguish them from the ZnO peaks. The first observation is that there are no noticeable ZnO peaks in the sample that was annealed at 300°C.

The peaks in the samples annealed at 400°C and 500°C are also not as defined as the ITO peaks. This would suggest that the crystal structure of the ZnO thin film is more amorphous than crystalline. It is also shown that the ratio between the (002) peak and the other ZnO peaks is highest for the sample annealed at 400°C.

HRSEM

High resolution SEM images were collected to get a better view of the surface features of the ZnO thin films. The machine was set to 3.0kV. The sample that was annealed at 300°C was coated with approximately 2 nm of iridium as to prevent excessive charging and to gain a higher quality image.

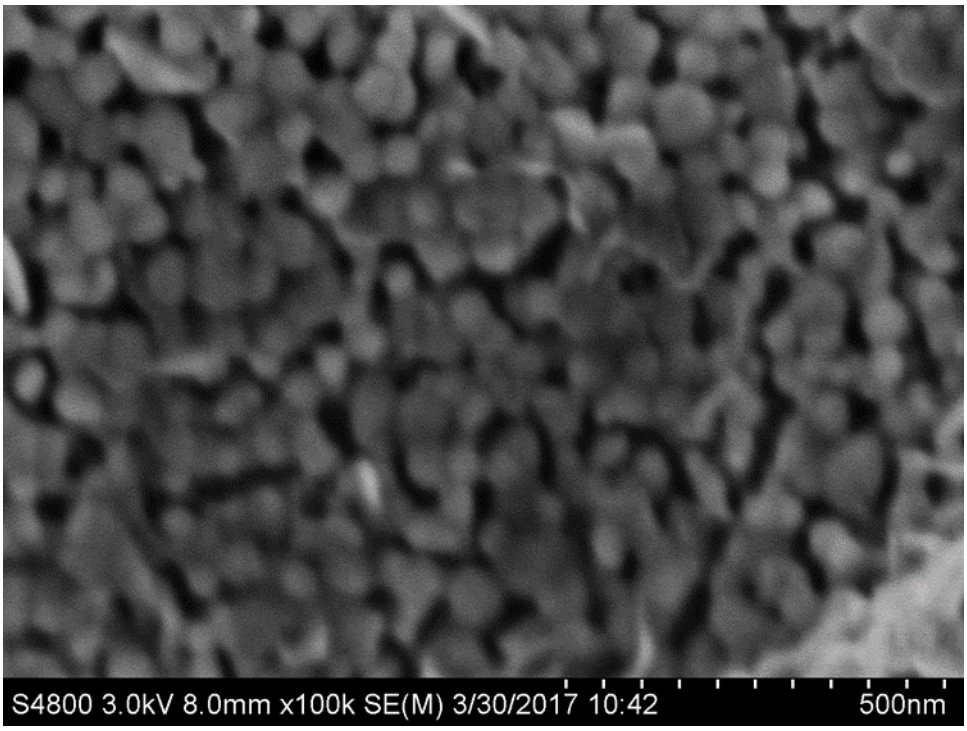

Figure 21: HRSEM image of a sample annealed at 500C. Taken at 100k magnification under 3.0kV electron beam

In figure 21, we can make out what appears to be nano particles. The sizes of these particles range from about 40 nm up to around 90 nm. XRD analysis approximated the crystal

size of this sample to be 57 nm. As the XRD results showed, there was no (002) favorability so the different sizes may be a result of different orientation of grain growth.

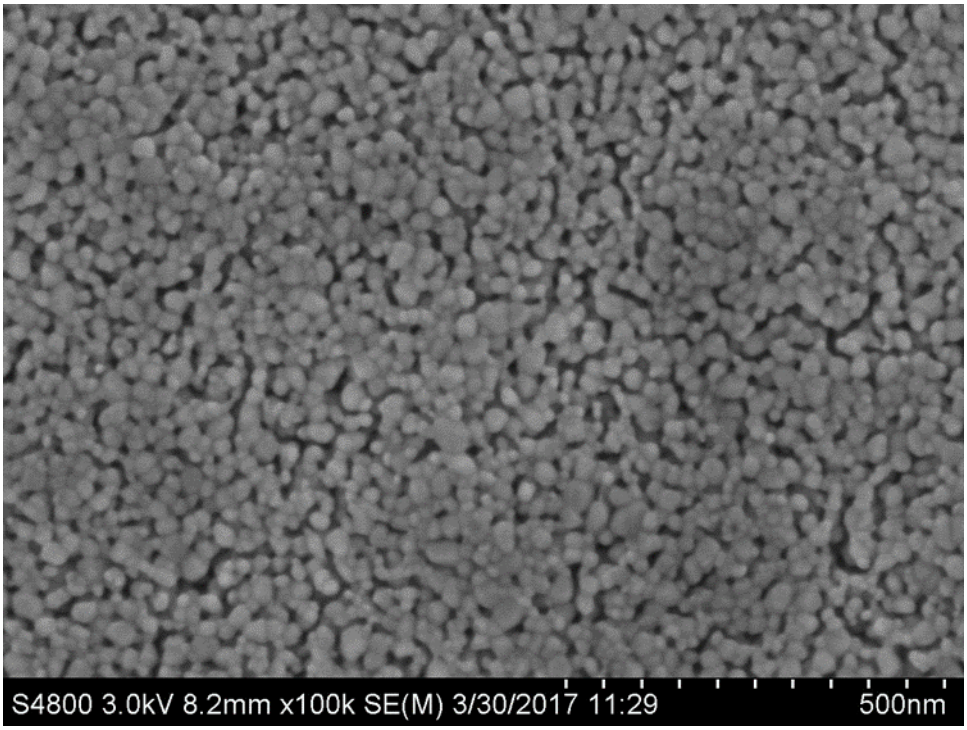

Figure 22: HRSEM image of a sample annealed at 400C. Taken at 100k magnification under 3.0kV electron beam

In Figure 22, we can see similar particles that were observed in the sample annealed at 500°C. The size of the larger particles is about 40 nm. This is similar to the approximate size determined in XRD analysis of 33.5 nm. XRD analysis also showed more preferred (002) growth. This image supports this as the distribution of particle size is bunched closer to around 35 nm. There are also fewer gaps between the particles relative to 500°C sample.

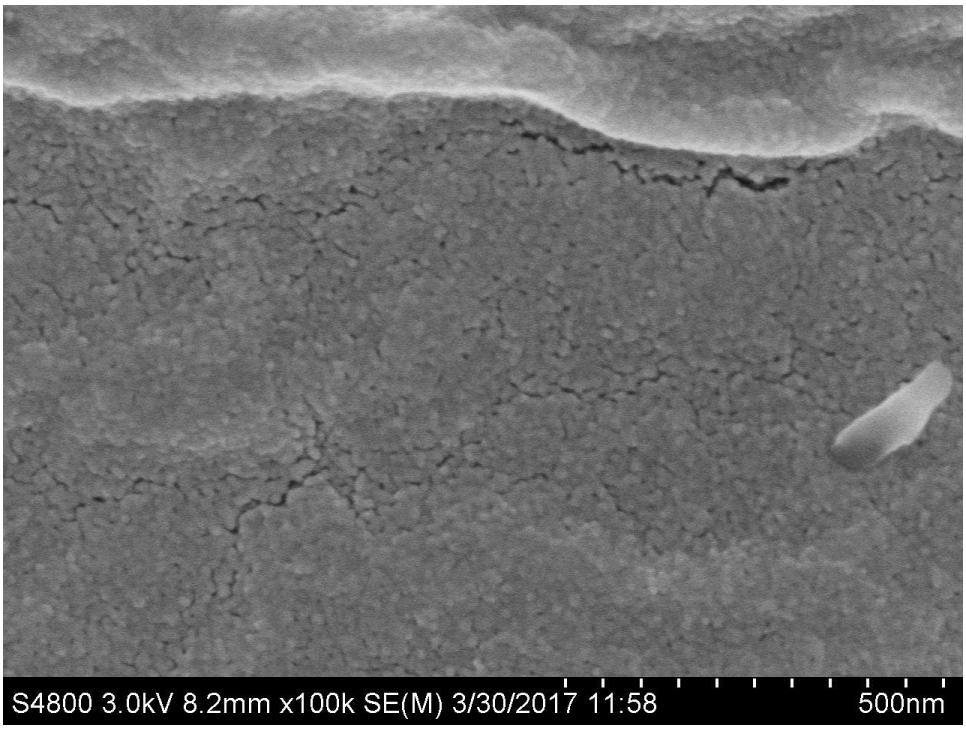

Figure 23: HRSEM image of a sample annealed at 300C. Taken at 100k magnification under 3.0kV electron beam

In figure 23, the individual particles appear to have morphed into a single, large, and interconnected structure. This could potentially support the result from the XRD test that this film is an entirely amorphous structure. There are still gaps present in the film but they appear to be in the form of cracks rather than gaps between the particles.

Summary

Samples annealed at 300°C produced a continuous, amorphous crystal structure with cracks appearing between the boundaries of different surface features. Samples annealed at 400°C and 500°C produced individual single crystal nano particles. Compared to the samples annealed at 400°C, samples annealed at 500°C had a low quantity but larger crystals. The net result was a larger gap, or void between the particles.

Discussion

As the annealing temperature is increased, XRD analysis shows a trend from an amorphous crystal structure, to the beginning of (002) grain growth, and then finally grain grow from all three of the major ZnO peaks. Although the specific parameters of chemical solution, pre-heat temperature and post-heat temperature range, has never been studied; these results do seem reasonable.

The HRSEM images did produce interesting results. The change between an amorphous, continuous structure to seemingly individual nanoparticles would indicate a critical temperature at which crystallization would occur. This transformation of surface features is never discussed in publication but is very important. The gaps in the particles support the theory that the films being produced are not a continuous film.

Future work

Both the pre-heat and post-heat temperatures have an effect on the grain formation. The effect of both is not straight forward as they each influence the grain growth in different ways. The pre-heat temperature will determine the grain seeds' size, quantity, and geography. The post-heat temperature will arranged the seeds into the final crystal structure. A more detailed analysis of the relationships between these two parameters should be studied. It may have to be done through the brute force of trial and error, as evaluating the crystal seeds after annealing may be difficult to do. This is due to unannealed samples not being conductive enough for SEM. This conductivity problem may be compounded by the potential size of the sample films; requiring a very high magnification to view.

References

A.E. Jimenez-Gonzalez, J. S.-P. (1998). Optical and electrical characteristics of aluminum-doped ZnO thin films prepared by solgel technique. *Journal of Crystal Growth volume*, 430-438.

B.K. Choi, D. C. (2006). Optical characterization of ZnO thin films deposited by Sol-gel method. *Journal of Material Science: Materials in Electronics volume 17*, 1011-1015.

D. Bao, H. G. (1998). Sol-gel-derived c-axis oriented ZnO thin films. *Thin Solid Films volume 312*, 37-39.

G.T. Delgado, C. Z. (2009). Optical and structural properties of the sol–gel-prepared ZnO thin films and their effect on the photocatalytic activity. *Solar Energy Materials and Solar Cells*, 55-59.

H.Y. Bae, G. C. (1999). Electrical and reducing gas sensing properties of ZnO and ZnO–CuO thin films fabricated by spin coating method. *Sensors and Actuators B: Chemical volume 55*, 47-54.

J. Wang, Y. Q. (2007). A self-assembly mechanism for sol-gel derived ZnO thin films. *Smart Material and Structures volume 16*, 2673-2679.

L.Y. Lin, D. K. (2009). Effect of annealing temperature on the tribological behavior of ZnO films prepared by sol–gel method. *Thin Solid Films volume 517*, 1690-1700.

M. Wang, E. K. (2006). Influence of annealing temperature on the structural and optical properties of sol–gel prepared ZnO thin films. *Physica status solidi A volume 203*, 2418-2425.

M. Wang, J. W. (2006). Effect of preheating and annealing temperatures on quality characteristics of ZnO thin film prepared by sol–gel method. *Materials Chemistry and Physics volume 97*, 219-225.

M.P. Bole, D. P. (2009). Effect of annealing temperature on the optical constants of zinc oxide films. *Jopurnal of Physics and Chemsitry of Solids volume*, 466-471.

M.W. Zhu, J. X.-S. (2008). Heat-activated structural evolution of sol-gel-derived ZnO thin films. *Journal of Crystal Growth volume 310*, 816-823.

Y. Caglar, S. I. (2009). Influence of heat treatment on the nanocrystalline structure of ZnO film deposited on p-Si. *Journal of Alloys and Compounds volume 481*, 885-889.

Znaidi, L. (2010). Sol-gel deposited ZnO thin films: A review. *Material Science and Engineering B.*

Chapter 5: Effect of cooling rate on crystal structure and surface properties

Overview

The effect of the cooling rate on the final grain formation and surface features was analyzed by XRD and HRSEM.

Introduction

The processing of zinc oxide (ZnO) thin films by sol-gel has many parameters to consider (Znaidi, 2010). The parameters include the chemistry and preparation of the solution, the type of substrate used, whether to utilize spin coating, doctor blade, or dip coating, the temperatures for the pre-heat or post-heat, and even the post-heat atmosphere to be analyzed to some degree (Y. Caglar, 2009) (S. Fujihara, 2001) (M.W. Zhu, 2008) (M.P. Bole, 2009) (M. Wang J. W., 2006) (M. Wang E. K., 2006) (L.Y. Lin, 2009) (H.Y. Bae, 1999) (G.T. Delgado, 2009) (G. Srinivasan, 2008) (D. Bao, 1998) (C. Shaoqaing, 2005) (B.K. Choi, 2006) (A.E. Jimenez-Gonzalez, 1998). In addition to these parameters, there does appear to be a lot of unaccounted variables that are unresearched.

In material processing at high temperatures, the cooling rate is very important to the properties of the final product being made. The effect of the cooling rate of sol-gel derived ZnO thin films is not discussed in the literature. Moreover, publications do not mention the cooling rates that are used in their studies. Unknown variables, such as these, add to the difficulty of reproducing results.

The electrical properties of ZnO thin films, produced through preliminary work, proved difficult to measure. For reference, the resistance of a typical commercially bought ITO glass

slide can be measure with a multimeter. Although this simple test is not highly reliable, it does show continuity of the thin film in the X-Y plane.

Since the ZnO thin films produced through preliminary work failed to produce expected results via the simple multimeter test, it was thought that these thin films lacked continuity. It was theorized that the thermal shock experienced by the thin film after annealing contributed to cracks in or discontinuity of the film. The second step in determining the different possible variables contributions to film continuity was to adjust the cooling rate of the samples from their annealing temperatures.

Synthesis and processing

The solution was prepared by adding 1.646g of zinc acetate dihydrate (ZnAcO) and 10mL of 200 proof ethanol (EtOH) to an Erlenmeyer flask. Some of the ZnAcO dissolved immediately but much of it remained as undissolved salts. Next, 0.433g of monoethanolamine (MEA) was added gravimetrically and the remaining ZnAcO fully dissolved to produce a clear solution. Then, the entire solution was placed on a hot plate set to 60°C and stirred at 250 rpm for one hour. Finally, the solution was covered with parafilm and stored in a dry, dark place and allowed to age at room temperature for 24 hours.

For this research, ITO coated slides were used in place of standard glass slides. The ITO coated glass microslides 3" x 1" were prepared by first cutting and sectioning them into three, 1" x 1" slides. They were then marked for identification on the reverse side of the surface to be coated. This was done so that the etching did not disturb the application of the solution. Slides were then hand washed with dish soap and then placed in a dilute nitric acid bath for ten minutes.

They were then rinsed off with deionized water (DI) and ethanol, and then dried in a 100°C oven for ten minutes.

Samples were then prepared by taking the cleaned glass substrates out of the oven and placed on the spin coater. Scotch tape was used to cover approximately half of the samples. As the sample was rotating, 3-4 drops of the solution were applied to the substrate. The sample was spun at 3000 rpm for 30 seconds. The scotch tape was removed from the sample before it was placed in a 100°C oven. After the samples were allowed to dry for about seven minutes, a new piece of scotch tape was replaced where the old piece was. The tape was replaced due to at the elevated temperature of the oven; a portion of the adhesive from the tape would remain on the sample as an impurity.

The final three sets of samples were made by repeating the above process four times in order to create multiple coats. The first set was placed in an oven at 300°C, the second at 400°C and the last set at 500°C. After the samples were annealed at their respective temperatures for one hour the furnace was turned off and allowed to cool off naturally.

Characterization

XRD Analysis

Structural analysis of the samples was carried out by x-ray diffraction. Before the samples were tested, a corundum standard was run and the accuracy of the machine was verified. The parameters of the machine were 40 kV and 40mA with a CuKa1 source with a wave length of 1.54nm. The tests were run at 40 mA and kV between 30° and 40° two-theta. This narrow and small angle range was chosen to analyze the three major peaks, (100), (002), (101) for (ZnO). Figures 24, 25, and 26 show the comparison of the XRD graphs between samples annealed at the same temperature but cooled at different rates.

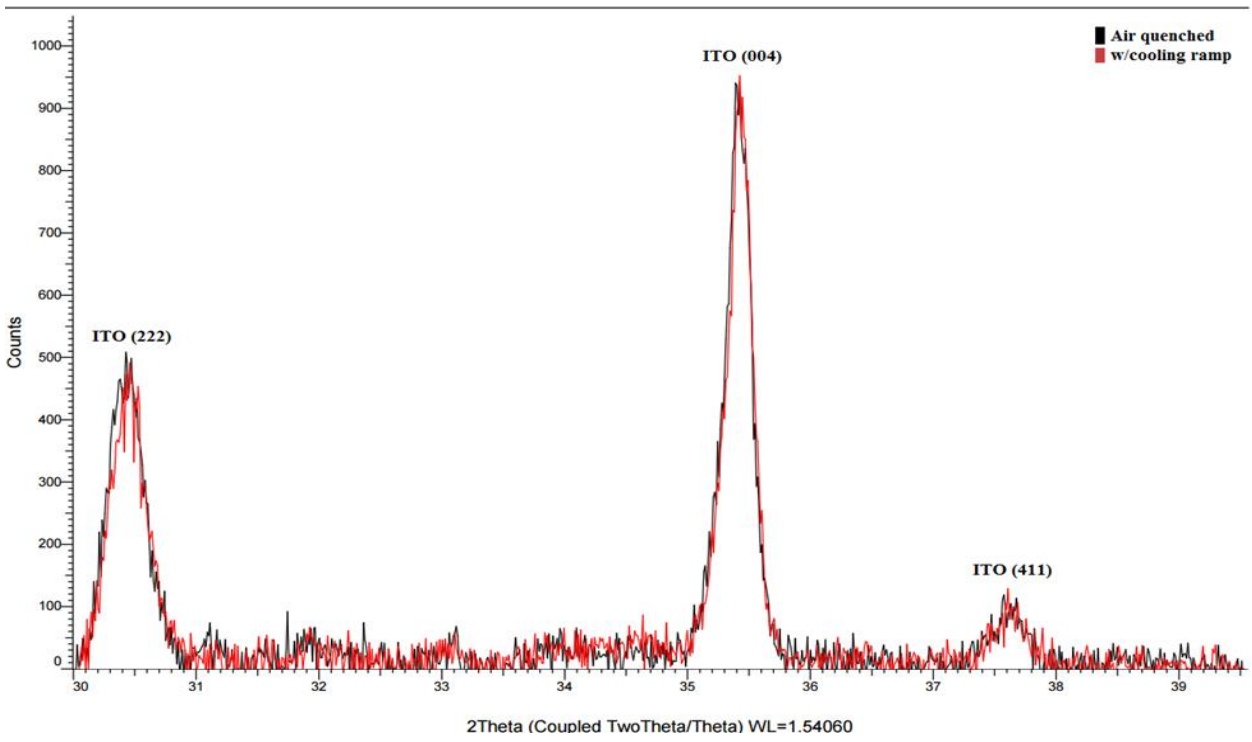

Figure 24: Comparative XRD analysis of samples annealed at 300°C and cooled at different rates

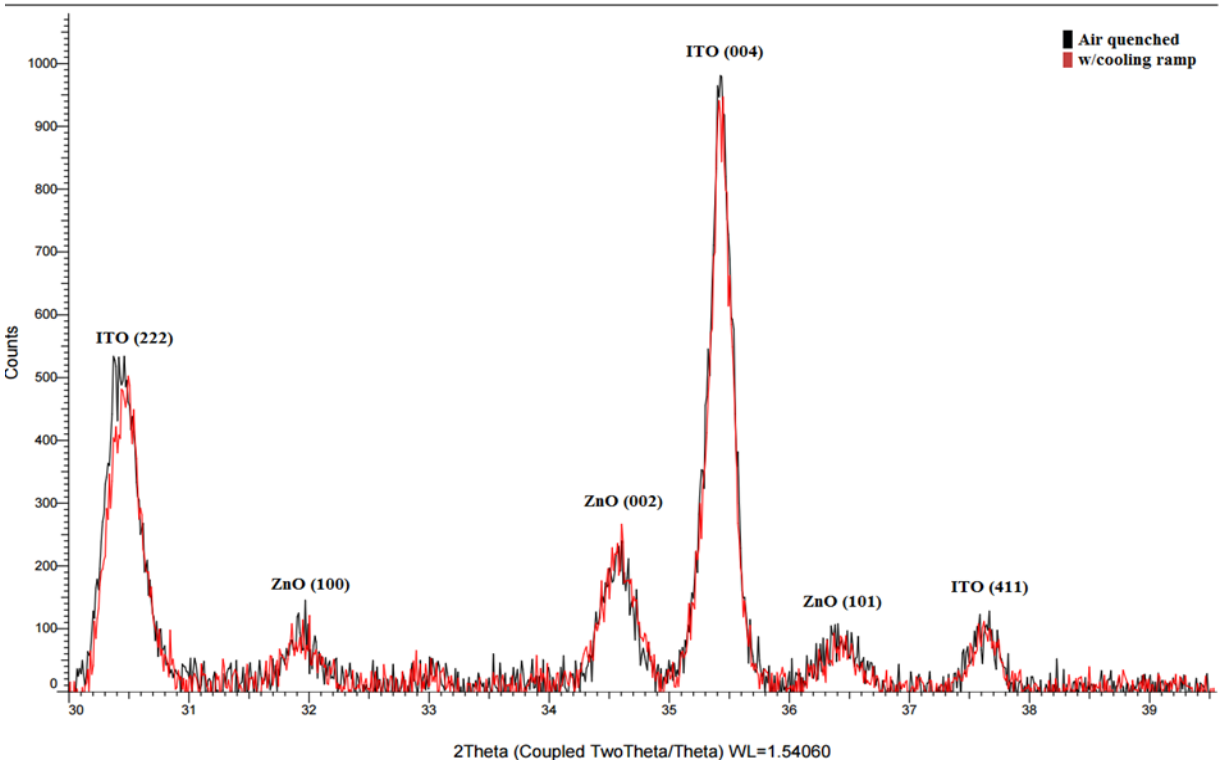

Figure 25: Comparative XRD analysis of samples annealed at 400°C and cooled at different rates

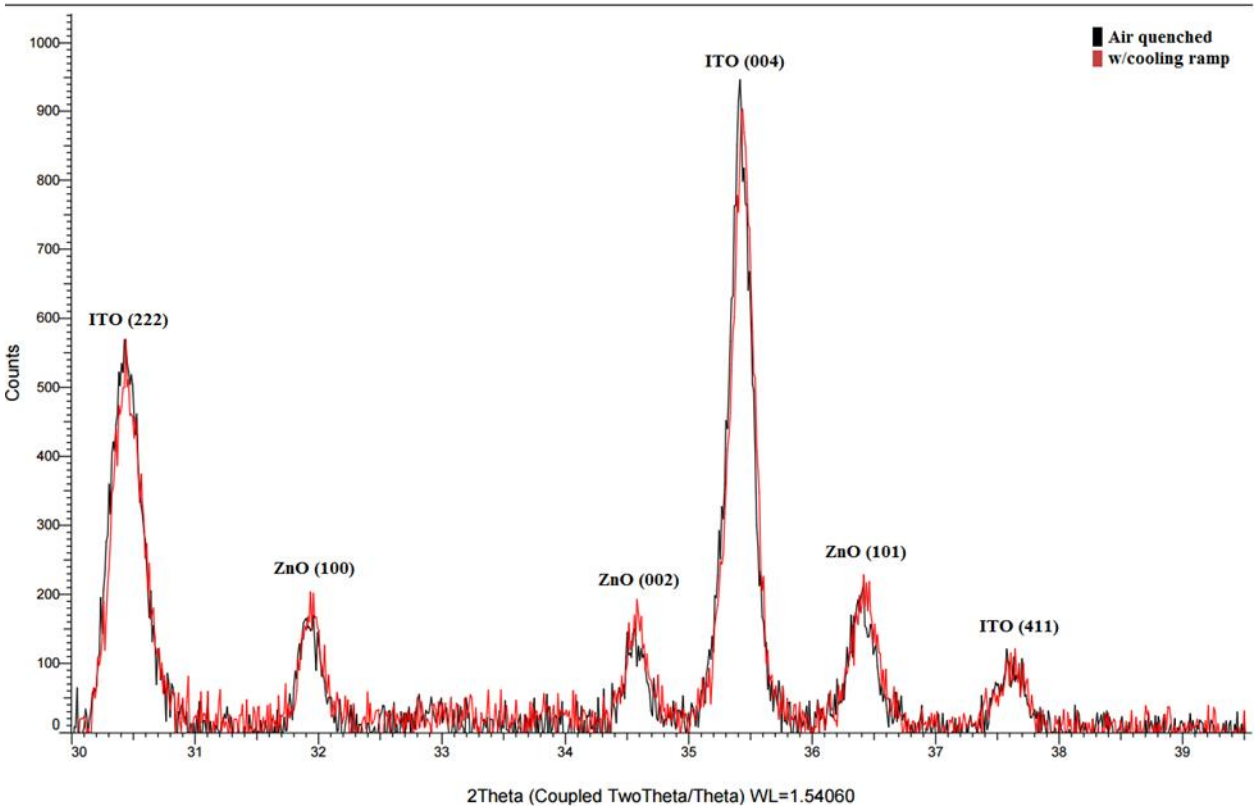

Figure 26: Comparative XRD analysis of samples annealed at 500°C and cooled at different rates

The general analysis of the samples that were air quenched also applies for the samples that were cooled down slower. The lack of ZnO peaks at 300°C, signify an amorphous crystal structure. The (002) preferential grain growth at 400°C is still present. In addition, the (002) grain preference no longer exists at 500°C is reproduced. The only divergent result noted in the XRD analysis is increased grain size in the samples that cooled off at a slower rate.

HRSEM

High resolution SEM images were collected to get a better view of the surface features of the ZnO thin films. The machine was set to 5.0kV. The sample that was annealed at 300°C was

coated with approximately 2 nm of iridium as to prevent excessive charging and to gain a higher quality image.

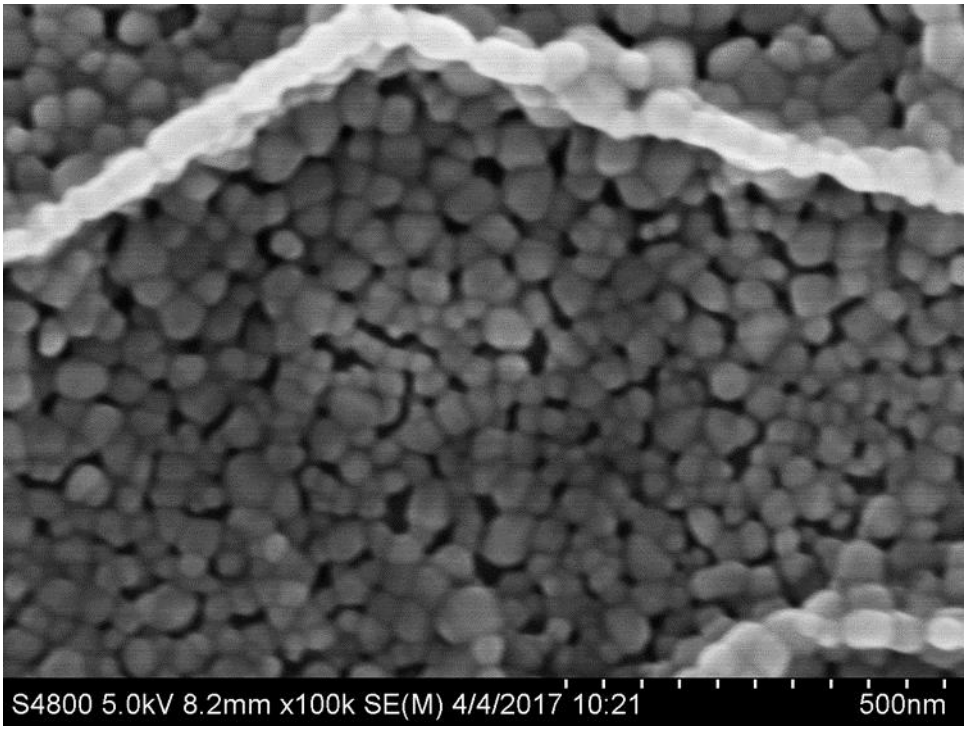

Figure 27: HRSEM image of a sample annealed at 500C and cooled gradually. Taken at 100k magnification under 5.0kV electron beam

Figure 27 shows similar particulates as seen with the air quenched samples annealed at 400°C and 500°C. A typical particulate size here is about 65 nm which is comparable to the XRD approximate of 63 nm. In contrast to the equivalently large particles, smaller gaps formed between the particles cooled at the slower rate relative to the air quenched samples at the same temperature.

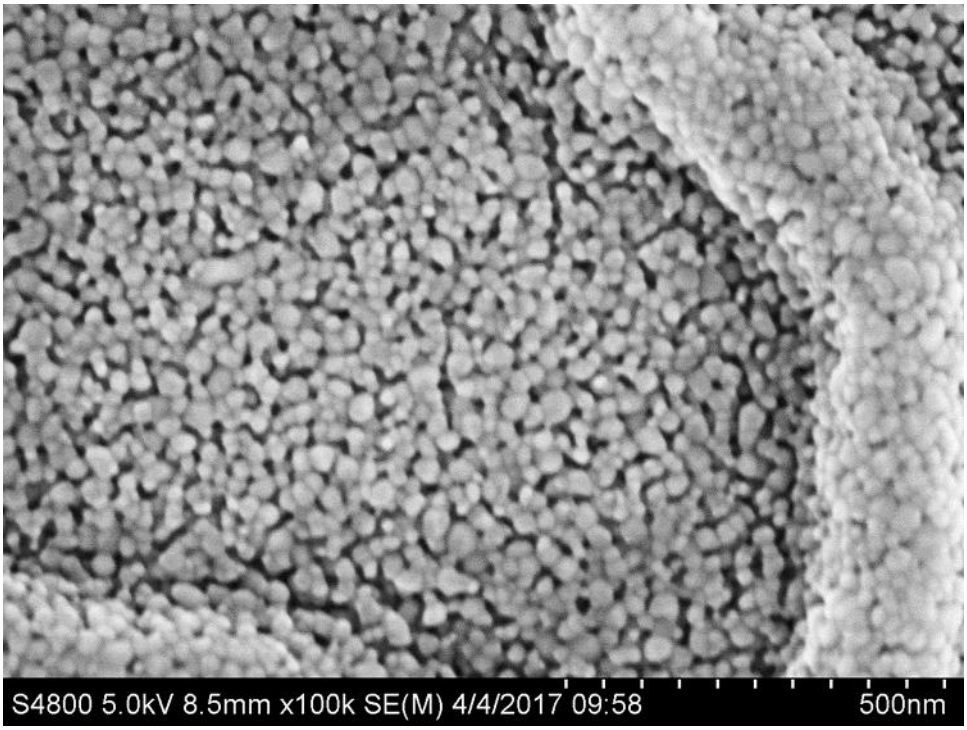

Figure 28: HRSEM image of a sample annealed at 400C and cooled gradually. Taken at 100k magnification under 5.0kV electron beam

Figure 28 shows a very similar crystal structure to the air quenched sample that was also annealed at 400°C. The XRD analysis indicated the grain size increase from 33.5 to 35.9 nm for the sample with the cooling ramp. This difference would be difficult to notice between the samples as the images indicate. There also does not appear to be a difference in the size or quantity of the gaps between the particles.

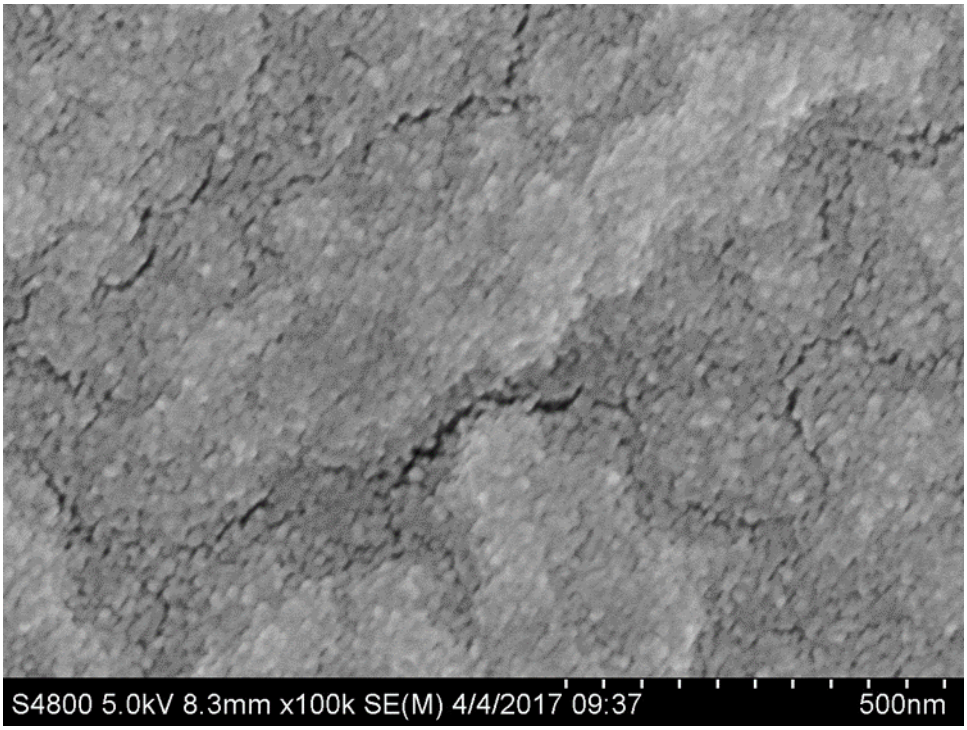

Figure 29: HRSEM image of a sample annealed at 300C and cooled gradually. Taken at 100k magnification under 5.0kV electron beam

Figure 29 shows individual particles have clumped up to create a single, continuous structure. This result is similar to the sample that was air quenched. The above figure reinforces the XRD result, suggesting a more amorphous crystalline structure. An increased number of cracks on the surface are shown in the image.

Summary

For samples annealed at 500°C, XRD and HRSEM analysis showed that those samples that were allowed to cool more slowly had the same quantity, but large sized individual crystals; resulting in smaller gaps between them.

For samples annealed at 400°C, XRD and HRSEM showed almost no noticeable difference between the samples cooled at different rates.

At 300°C, HRSEM showed that the samples that were cooled down slowly resulted in more cracks, in general, on the surface. These results are completely opposite of what should be expected and should attempted to be reproduced at a later date in order to confirm the results.

Discussion

When comparing the samples by XRD, the only noticeable difference between the crystal structures of each sample is the larger crystal sizes slower cooled samples. As to be expected, with a lower degree of undercooling, there are larger grain sizes.

HRSEM analysis for samples annealed at 500°C shows approximately same number of nanoparticles per unit area regardless of cooling rate. Although the number of particles remains constant, the slower cooling rate results in grains becoming larger and gaps between the nanostructures becoming smaller. This indicates that the cooling rate does have a significant effect on the continuity of the ZnO thin film.

XRD analysis for the samples annealed at 400°C shows a nearly identical structure. There is also no significant change in the size of the crystals with different cooling rate. HRSEM shows that there is approximately the same count of nanoparticles per unit area between samples, resulting in nearly identical samples.

For the samples annealed at 300°C, HRSEM images show an increase in cracks for samples that were cooled slowly, counter to what was expected. The samples were inspected at multiple locations and the same results appeared. However, the sites that were examined may not be representative of the rest of the film. Further analysis should be done on future samples to confirm these results.

This research shows that the cooling rate is an important factor in the formation of ZnO thin films. The method of cooling should be included amongst the variables in future research to allow for a greater chance of reproducibility of results.

Future work

As this is the first known comparison of cooling rates to this author, this topic has room for expansion. Two cooling rates chosen for this this research; show that the cooling rate does have an impact on the ZnO thin films. The next step would be to explore slower cooling rates and to determine if a trend is discernable. Perhaps then an ideal cooling rate can be determined that strikes an appropriate balance between sample performance and processing cost.

This topic was chosen to attempt to solve a problem and study a topic that has not been previously discussed. It represents another parameter that must be controlled, or accounted for, in research on this topic. Researchers should be encouraged to look for unknown or unaccounted variables that could cause variation in results. This will allow Sol-gel processed ZnO thin films to come into maturity as a field of research.

References

A.E. Jimenez-Gonzalez, J. S.-P. (1998). Optical and electrical characteristics of aluminum-doped ZnO thin films prepared by solgel technique. Journal of Crystal Growth volume, 430-438.

B.K. Choi, D. C. (2006). Optical characterization of ZnO thin films deposited by Sol-gel method. Journal of Material Science: Materials in Electronics volume 17, 1011-1015.

C. Shaoqaing, Z. J. (2005). Nanocrystalline ZnO thin films on porous silicon/silicon substrates obtained by sol–gel technique. Applied Surface Science volume 241, 384-391.

D. Bao, H. G. (1998). Sol-gel-derived c-axis oriented ZnO thin films. Thin Solid Films volume 312, 37-39.

G. Srinivasan, N. G. (2008). Influence of post-deposition annealing on the structural and optical

properties of ZnO thin films prepared by sol–gel and spin-coating method. Superlatticies and Microstructures volume 43, 112-119.

G.T. Delgado, C. Z. (2009). Optical and structural properties of the sol–gel-prepared ZnO thin films and their effect on the photocatalytic activity. Solar Energy Materials and Solar Cells, 55-59.

H.Y. Bae, G. C. (1999). Electrical and reducing gas sensing properties of ZnO and ZnO–CuO thin films fabricated by spin coating method. Sensors and Actuators B: Chemical volume 55, 47-54.

L.Y. Lin, D. K. (2009). Effect of annealing temperature on the tribological behavior of ZnO films prepared by sol–gel method. Thin Solid Films volume 517, 1690-1700.

M. Wang, E. K. (2006). Influence of annealing temperature on the structural and optical properties of sol–gel prepared ZnO thin films. Physica status solidi A volume 203, 2418-2425.

M. Wang, J. W. (2006). Effect of preheating and annealing temperatures on quality characteristics of ZnO thin film prepared by sol–gel method. Materials Chemistry and Physics volume 97, 219-225.

M.P. Bole, D. P. (2009). Effect of annealing temperature on the optical constants of zinc oxide films. Jopurnal of Physics and Chemsitry of Solids volume, 466-471.

M.W. Zhu, J. X.-S. (2008). Heat-activated structural evolution of sol-gel-derived ZnO thin films. Journal of Crystal Growth volume 310, 816-823.

S. Fujihara, C. S. (2001). Crystallization behavior and origin of c-axis orientation in sol–gel-derived ZnO:Li thin films on glass substrates. Applied Surface Science volume 180, 341-350.

Y. Caglar, S. I. (2009). Influence of heat treatment on the nanocrystalline structure of ZnO film deposited on p-Si. Journal of Alloys and Compounds volume 481, 885-889.

Znaidi, L. (2010). Sol-gel deposited ZnO thin films: A review. Material Science and Engineering B.

Chapter 6: Future Work

The lack of discussion of the cooling rate is an example of an unknown or unaccounted for parameter in the process of sol-gel derived ZnO thin films. There are other parameters that are generally not controlled or mentioned in research such as atmospheric environment for both solution application and sample annealing,

The individual samples prepared throughout this research were prepared over several months. This means the humidity and temperature of the room was undoubtedly different. Although the difference was not measured and could be considered relatively small, it is currently unknown whether these things affect the final film. This is something that should be considered as a future research topic to determine if such parameters need to be tightened to ensure a consistent quality.

Publications that experiment with novel processing techniques such as substrate temperature (R.K. Gupta, 2010), shed light on other parameters that must be considered or tightened in processing technique. The substrate temperature is something that can change between the operators producing the cells where a quicker operator will move the cells from the drying furnace to the spin coater quicker, resulting in a different temperature.

Experimenting with unique processing parameters should also be encouraged as it might lead to results that demonstrate better performance. One example, the paper by Lee et al produced samples that were annealed under different atmospheres of gas (J.H. Lee, 2003). Another is the publication by Natsume et al (Y. Natsume, 2000) that used a slightly modified processing order to produce their films, depicted in Figure 30 taken from their work. Whether

this was intentional or not, small changes like this could result in thin films with different crystal structures

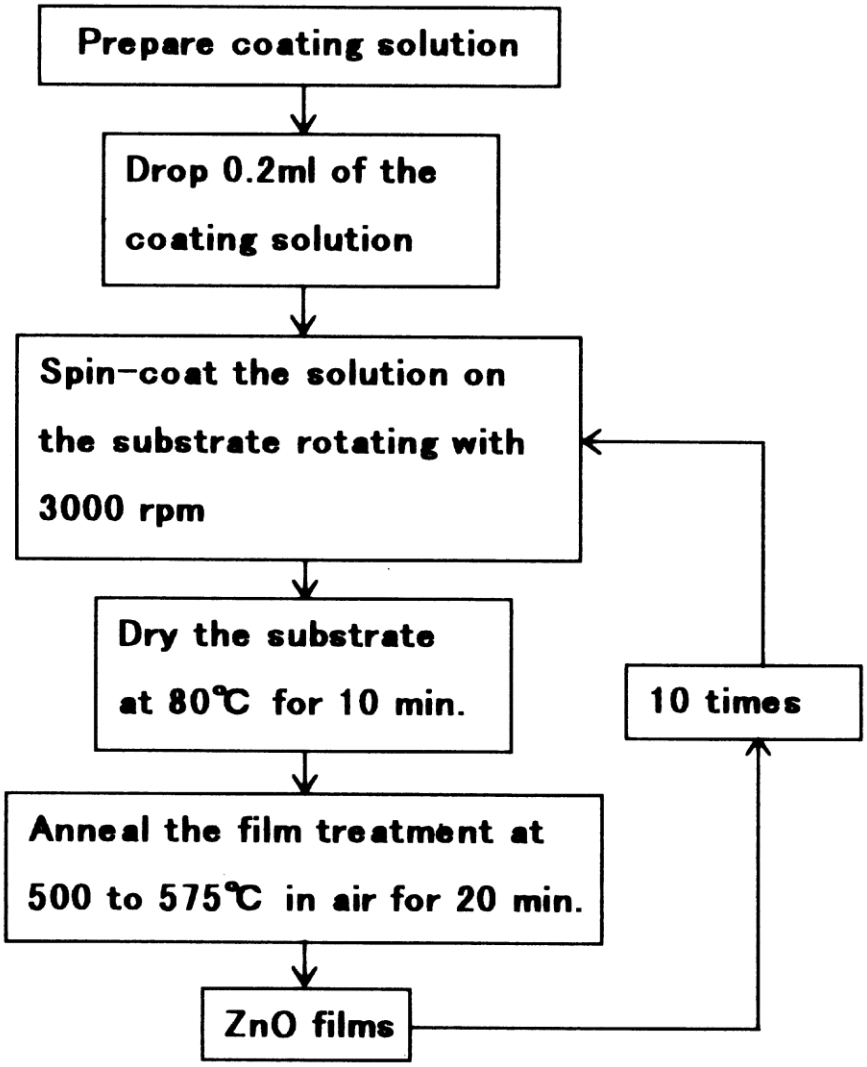

Figure 30: Image detailing an alternative processing procedure

On top of the research being done to better understand the processing parameters and optimizing the ZnO thin films, further characterization must be done to determine the viability of these films to be used in various applications this includes optical and electrical characterization such and UV-Vis, 4-point probe, and hall effect measurements. This can also be expanded to novel characterization techniques.

Sol-gel synthesis was the main focus of this research and spin coating was simply used as a vessel to produce samples as a proof of concept. However, there are some major draw backs to spin-coating. The nature of this processing technique severely limits the size of samples and rate of production. For making small amounts of 1" x 1" samples, this is ok. But for scalability purposes, this is simply unacceptable.

Another drawback to spin coating is that is has very inefficient resource management. A good portion of the solution that is deposited onto the spinning slides is flung off the edges. Dip coating is an alternative method for applying the solution onto a substrate. This of course would come with needing to modify its own unique processing parameters such as substrate feed and withdrawal rate. Dip-coating is not as limited by sample size and scalability as spin-coating is.

Other processing techniques such as Roll-to-Roll processing could be adapted to work with sol-gel. There are several other potential applications that will each have their own advantage and drawbacks and may have to be considered on a case by case basis. The important thing for researchers is to focus on the strengths that these processes bring to sol-gel production.

Organic photovoltaic (OPV) solar cells often have stability issues due to the degradation of the photo active layer (V.L. Dalal, 2012). Several factors that contribute to this degradation are UV light exposure and penetration of water and oxygen into the photo active layer (M. Jorgensen, 2008) (K. Kawano, 2006). ZnO, with a bandgap of 3.37 eV is already used as a UV filter.

Future research can focus on ZnO's ability to prevent water and oxygen from getting through to the active layer of an OPV. ZnO is not soluble in water so there is a good chance that it would be a good protective layer to keep water out. It may seem counter intuitive to use an

oxide thin film to prevent oxygen from getting to the active layer of an OPV but there are good reasons why it will help.

The oxygen inside of the zinc oxide crystal structure is at a very thermodynamically favorable spot. It would require a high amount of energy for the oxygen to move out of its crystal location. Furthermore, Fick's law of diffusion is partially dependent on the concentration gradient of the element in questions. Since ZnO will have a higher oxygen concentration than non-oxide electrodes and buffer layers, this will increase its chances to be able to prevent oxygen from getting to the active layer.

There are other out of the ordinary properties that can be studied such as thermal conductivity and radiation hardness. Expanding the characterization of ZnO thin films to include novel properties will provide more information of its potential. This will increase interest in the material and expand range of applications that it can be used in.

References

J.H. Lee, K. K. (2003). Electrical and optical properties of ZnO transparent conducting films by the sol–gel method. Journal of Crystal Growth volume 247, 119 125.

K. Kawano, R. P. (2006). Degradation of organic solar cells due to air exposure. Solar Energy Materials and Solar Cells volume 90, 3520-3530.

M. Jorgensen, K. M. (2008). Stability/degradation of polymer solar cells. Solar Energy Materials and Solar Cells volume 92, 686-714.

P. Singh, N. R. (2012). Temperature dependence of solar cell performance- an analysis. Solar Energy Materials and Solar Cells volume 101, 36-45.

R.K. Gupta, K. G. (2010). Effect of substrate temperature on structural and optoelectrical properties. Physica E.

V.L. Dalal, R. M. (2012). Stability of organic solar cells. Reliability Physics Symposium.

Y. Natsume, H. S. (2000). Zinc oxide films prepared by sol-gel spin-coating. Thin Solid Films volume 372, 30-36.

References

(n.d.).

A. Hernandez Battez, R. G. (2008). CuO, ZrO2 and ZnO nanoparticles as antiwear additive in oil lubricants. *Wear volume 265*, 422-428.

A. Mang, K. R. (1995). Band gaps, crystal-field splitting, spin-orbit coupling, and exciton binding energies in ZnO under hydrostatic pressure. *Solid State Communications*, 251-254.

A. Tsukazaki, A. O. (2005). Repeated temperature modulation epitaxy for p-type doping and light-emitting diode based on ZnO. *Nature materials 4*, 42-46.

A.A. Ralib, A. N. (2016). A study on controllable aluminium doped zinc oxide patterning by chemical etching for MEMS application. *Microsystem technologies*.

A.E. Jimenez-Gonzalez, J. S.-P. (1998). Optical and electrical characteristics of aluminum-doped ZnO thin films prepared by solgel technique. *Journal of Crystal Growth volume*, 430-438.

B. Sang, Y. N. (2003). MOCVD-ZnO windows for 30 cmx 30cm CIGS-based modules. *Solar Energy Materials and Solar Cells volume 75*, 179-184.

B.K. Choi, D. C. (2006). Optical characterization of ZnO thin films deposited by Sol-gel method. *Journal of Material Science: Materials in Electronics volume 17*, 1011-1015.

C. H. Park, S. B.-H. (2002). Origin of p-type doping difficulty in ZnO: The impurity perspective. *Physical Review B*.

C. Shaoqaing, Z. J. (2005). Nanocrystalline ZnO thin films on porous silicon/silicon substrates obtained by sol–gel technique. *Applied Surface Science volume 241*, 384-391.

Chemicals, S. (2013, May 10). *Bubblers and Cylinders for CVD.ALD Precursor Handling*. Retrieved from azonano: http://www.azonano.com/article.aspx?ArticleID=3423

D. Bao, H. G. (1998). Sol-gel-derived c-axis oriented ZnO thin films. *Thin Solid Films volume 312*, 37-39.

D. C. Look, J. W. (1999). Residual Native Shallow Donor in ZnO. *Physics Review Letters 82*, 2552.

D. C. Reynolds, D. C. (1999). Valence-band ordering in ZnO. *Physical review B*, 2340.

D. I. Florescu, L. G. (2001). High spatial resolution thermal conductivity of bulk ZnO (0001). *Journal of Applied Physics volume 91* .

D.C. Reynolds, D. L. (1996). Optically pumped ultraviolet lasing from ZnO. *Solid State Communications volume 99*, 873-875.

D.J. Rogers, F. H. (2010). ZnO thin films and nanostructures for emerging optoelectronic applications. *Proceedings of the 12th Optoelectronic integrated Circuits*.

D.M. Bagnall, Y. F. (1997). Optically pumped lasing of ZnO at room temperature. *Applied Physics Letters volume 70*.

Eason, R. (2007). *Pulsed Laser Deposition of Thin Films.* New Jersey: John Wiley and Sons.

F. Tuomisto, K. S. (2005). Introduction and recovery of point defects in electron-irradiated ZnO. *Physical Review B 72*, 085206.

G. Srinivasan, N. G. (2008). Influence of post-deposition annealing on the structural and optical properties of ZnO thin films prepared by sol–gel and spin-coating method. *Superlatticies and Microstructures volume 43*, 112-119.

G.T. Delgado, C. Z. (2009). Optical and structural properties of the sol–gel-prepared ZnO thin films and their effect on the photocatalytic activity. *Solar Energy Materials and Solar Cells*, 55-59.

H. Me, Z. Z. (2014). High sensitive formaldehyde graphene gas sensor modified by atomic layer deposition zinc oxide films. *Applied physics letters volume 105*.

H. Sato, T. M. (1993). Transparent conducting p-type NiO thin Films prepared by magnetron sputtering. *Thin Solid Films volume 236*, 27-31.

H. Zeng, X. X. (2009). Template deformationtailored ZnOnanorod/nanowire arrays: full growth control and optimization of field-emission. *Advanced Functional Materials vol 19*, 3165-3172.

H.S. Chin, L. C. (2016). Crystal, optical, and electrical characteristics of transparent conducting gallium-doped zinc oxide films deposited on flexible polyethylene naphthalate substrates using radio frequency magnetron sputtering. *Materials Research Bulletin volume 79*, 90-96.

H.Y. Bae, G. C. (1999). Electrical and reducing gas sensing properties of ZnO and ZnO–CuO thin films fabricated by spin coating method. *Sensors and Actuators B: Chemical volume 55*, 47-54.

J. Hong, Y. H. (2012). Bicolor light-emitting diode based on Zinc oxide nanorod arrays and poly(2-methoxy,5-octoxy)-1,2-phenylenevinylene. *Journal of Electronic materials vol 41*, 431-436.

J. Livage, D. G. (2001). Sol-gel electrochromic coatings and devices: a review. *Solar Energy and Materials and Solar Cells volume 68*, 365-381.

J. Tate, M. J. (2002). p-Type oxides for use in transparent diodes. *Thin Solid films, volume 411*, Pages 119-124.

J. Wang, Y. Q. (2007). A self-assembly mechanism for sol-gel derived ZnO thin films. *Smart Material and Structures volume 16*, 2673-2679.

J.G.E. Gardeniers, Z. R. (1998). Preferred orientation and piezoelectricity in sputtered ZnO films. *Journal of applied physicsvolume 83*, 7844.

J.H. Lee, K. K. (2003). Electrical and optical properties of ZnO transparent conducting films by the sol–gel method. *Journal of Crystal Growth volume 247*, 119 125.

K. Kawano, R. P. (2006). Degradation of organic solar cells due to air exposure. *Solar Energy Materials and Solar Cells volume 90*, 3520-3530.

K. Yim, J. L. (2017). Property database for single-element doping in ZnO obtained by automated first-principle calculations. *Nature scientific reports 7*.

L.J. Mandalapu, Z. Y. (2006). Homojunction photodiodes based on Sb-dopedp-type ZnO for ultraviolet detection. *Applied Physics letters volume 88*.

L.Y. Lin, D. K. (2009). Effect of annealing temperature on the tribological behavior of ZnO films prepared by sol–gel method. *Thin Solid Films volume 517*, 1690-1700.

Leng, Y. (2013). In Y. Leng, *Materials Characterization: Introduction to Microscopic and Spectroscopic Methods* (pp. 47-82). Weinheim: Wiley-VCH.

Leng, Y. (2013). Scanning Electron Microscopy. In Y. Leng, *Materials Characterization: Introduction to Microscoping and Spectroscopic Methods* (pp. 127-160). Weinheim: Wiley-VCH.

Leng, Y. (2013). X-ray Spectroscopy for Elemental Analysis. In Y. Leng, *Materials Characterization: Introduction to Microscopin and Spectroscopic Methods* (pp. 191-219). Weinheim: Wiley-VCH.

M. Hu, E. P. (2000). Sol–Gel and Ultrafine Particle Formation via Dielectric Tuning of Inorganic Salt–Alcohol–Water Solutions. *Journal of Colloid and Interface Science volume 222*, 20-36.

M. Jorgensen, K. M. (2008). Stability/degradation of polymer solar cells. *Solar Energy Materials and Solar Cells volume 92*, 686-714.

M. Joseph, H. T. (1999). p-Type Electrical Conduction in ZnO Thin Films by Ga and N Codoping. *Japanese Journal of Applied Physics volume 38*.

M. Mickan, U. H. (2016). Room temperature deposition of homogeneous, highly transparent and conductive Al-doped ZnO films by reactive high power impulse magnetron sputtering. *Solar Energy Materials and Solar Cells volume 157*, 742-749.

M. Ohyyama, H. K. (1997). Sol-gel preparation of ZnO films with extremely preferred orientation along (002) plane from zinc acetate solution. *Thin Solid films volume 306*, 78-85.

M. Wang, E. K. (2006). Influence of annealing temperature on the structural and optical properties of sol–gel prepared ZnO thin films. *Physica status solidi A volume 203*, 2418-2425.

M. Wang, J. W. (2006). Effect of preheating and annealing temperatures on quality characteristics of ZnO thin film prepared by sol–gel method. *Materials Chemistry and Physics volume 97*, 219-225.

M. Wang, J. W. (2006). Effect of preheating and annealing temperatures on quality characteristics of ZnO thin film prepared by sol–gel method. *Materials Chemistry and Physics volume 97*, 219-225.

M.N. Kamalasanan, S. C. (1996). Sol-gel synthesis of ZnO thin films. *Thin Solid Films volume 288*, 112-115.

M.P. Bole, D. P. (2009). Effect of annealing temperature on the optical constants of zinc oxide films. *Jopurnal of Physics and Chemsitry of Solids volume*, 466-471.

M.S. Wagh, G. J. (2006). Modified zinc oxide thick film resistors as NH3 gas sensor. *Sensors and Actuators B: Chemical volume 115*, 128-133.

M.W. Zhu, J. X.-S. (2008). Heat-activated structural evolution of sol-gel-derived ZnO thin films. *Journal of Crystal Growth volume 310*, 816-823.

Minami, T. (2005). Transparent conducting oxide semiconductors for a transparent electrodes. *Institute of physics publishing*.

P. Singh, N. R. (2012). Temperature dependence of solar cell performance- an analysis. *Solar Energy Materials and Solar Cells volume 101*, 36-45.

Pierre, A. C. (1998). *Introduction to Sol-Gel Processing.* New York: Springer.

Pierson, H. O. (1999). *Handbook of Chemical Vapor Deposition.* New York: Noyes Publication.

Q. A. Drmosh, S. (n.d.).

Q.A.Drmosh, S. R. (2012). Crystalline nanostructured Cu doped ZnO thin films grown at room temperature by pulsed laser deposition technique and their characterization. *Applied Surface Science volume 270*, 104-108.

R. Mannam, S. E. (2015). Zn-vacancy induced violet emission in p-type phosphorus and nitrogen codoped ZnO thin films grown by pulsed laser deposition. *Applied Surface Science volume 347*, 96-100.

R. Ondo-Ndong, G. F.-D. (2003). Electrical properties of zinc oxide sputtered thin films. *Microelectronics Journal volume 34*, 1087-1092.

R.K. Gupta, K. G. (2010). Effect ofsubstratetemperatureonstructuralandoptoelectricalproperties. *Physica E*.

Rao, B. B. (2000). Zinc Oxide ceramic semi-conductor gas sensor for ethanol vapour. *Materials Chemistry and Physics volume 64*, 62-65.

S. B. Zhang, S. -H. (2001). Intrinsic n-type versus p-type doping asymmetry and defect physics of ZnO. *Physics review b, volume 63*.

S. Chu, M. O. (2008). Electrically pumped ultraviolet ZnO diode lasers on Si. *Applied Physics Letters volume 93*.

S. Fujihara, C. S. (2001). Crystallization behavior and origin of c-axis orientation in sol–gel-derived ZnO:Li thin films on glass substrates. *Applied Surface Science volume 180*, 341-350.

S. Khosravi-Gandomani, R. Y.-S. (2013). Optical and electrical properties of p-type Ag-doped ZnO nanostructures. *Ceramics International*.

S. Shionoya, W. H. (2006). *Phosphor Handbook.* CRC Press.

S.M. Ali, W. F. (2015). Structural and optical properties of pure and Ag doped ZnO thin films obtained by sol-gel spin coating technique. *Material Science-Poland volume 33*, 601-605.

S.S. Shariffudin, M. H. (2012). Influence of drying temperature on the Structural, Optical, and Electrical properties of Layer-by-Layer ZnO nanoparticles seeded Catalyst. *Journal of Nanomaterials volume 2012, Article ID 359103*, 7.

SEM Technology. (n.d.). Retrieved from nanoimages: http://www.nanoimages.com/technology/

Stadler, A. (2012). Transparent Conducting Oxides-An up-to-date overview. *Materials vol 5*, 661-683.

T. Touam, F. B. (2015). Effect of silver doping on the structural, morphological, optical, and electrical properties of sol-gel deposited nanostructured ZnO thin films. *Optik 126*, 5548-5552.

T. Venkatesan, X. W. (1988). High-temperature superconductivity in ultrathin films of Y1Ba2Cu3O7−x. *Applied Physics Letters volume 54*.

T. Yamamoto, T. S. (2008). Characterization of ZnO piezoelectric films prepared by rf planar-magnetron sputtering. *Journal of Applied physics volume 51*.

Tedsanders. (2016, Febreuary 7). *Wikipedia: Pulsed laser deposition*. Retrieved from Wikipedia: https://en.wikipedia.org/wiki/Pulsed_laser_deposition#/media/File:Diagram_of_pulsed_laser_deposition.png

Thomas, D. (1960). The exciton spectrum of Zinc Oxide. *Journal of Physics and Chemistry of Solids volume 15*, 86-96.

Ü. Özgür, X. G.-J. (2006). Thermal conductivity of bulk ZnO after different thermal treatments. *Journal of Electronic Materials volume 35*, 550-555.

V. Srikant, D. C. (1998). On the optical band gap of zinc oxide. *Journal of applied physics*, 5447.

V.L. Dalal, R. M. (2012). Stability of organic solar cells. *Reliability Physics Symposium*.

W.S. Noh, J. L. (2016). Effect of oxygen pressure on the p-type conductivity of Ga, P co-doped ZnO thin film grown by pulsed laser deposition. *Ceramics International volume 42*, 4136-4142.

Walle, A. J. (2009). Fundamnetals of zinc oxide as a semiconductor. *Institute of physics*.

Wen-Jun Li, E.-W. S.-Z.-W. (May 1999). Growth mechanism and growth habit of oxide crystals. *Journal of Crystal Growth volume 203 issue 1-2*, 186-196.

What is Zinc oxide. (n.d.). Retrieved from What is Zinc oxide: http://whatiszincoxide.weebly.com/structure.html

Y. Caglar, S. I. (2009). Influence of heat treatment on the nanocrystalline structure of ZnO film deposited on p-Si. *Journal of Alloys and Compounds volume 481*, 885-889.

Y. Chen, D. B.-t. (1998). Plasma assisted molecular beam epitaxy of ZnO on c -plane sapphire: Growth and characterization. *Journal of Applied Physics volume 84* , 3912.

Y. Natsume, H. S. (2000). Zinc oxide films prepared by sol-gel spin-coating. *Thin Solid Films volume 372*, 30-36.

Y. Wang, T. W. (2014). Well-controlled wet etching of ZnO films using hydrogen peroxide solution. *Applied Surface Science volume 292*, 34-38.

Y. Yan, M. A.-J. (2006). Doping of ZnO by groub-IB elements . *Applied Physics Letters volume 89*, 181912.

Y. Yan, S. Z. (2001). Control of Doping by Impurity Chemical Potentials: Predictions for p-type ZnO. *Physical Review Letters volume 86*, 5723.

Y.R. Ryu, S. Z. (2000). Synthesis of p-type ZnO films. *Journal of Crystal Growth volume 216*, 330-334.

Y.R. Ryu, W. K. (2000). Fabrication of homostructural ZnO p–n junctions. *Journal of Crystal Growth*, 419-422.

Yanfa Yan, M. M.-J.-H. (2006). Doping of ZnO by hroup-1B elements. *Applied physics letters*.

Yanli Liu, Y. L. (2013). ZnO-Based Transparent Conductive Thin Films: Doping, Performance, and Processing. *Hindawi Publishing Corporation, Journal of Nanomaterials*.

Ylilammi, J. M. (2003). Piezoelectric ZnO films by r.f. sputtering. *Journal of material science: Materials in electronics volume 14*, 431-435.

Young-Sung Kim, W.-P. T.-J. (2005). Effect of preheating temperature on structural and optical properties of ZnO thin films by sol-gel process. *thin solid films 491*, 153-160.

Yu, P. C. (2010). *Fundamentals of Semiconductors.* Springer.

Zayat, D. L. (2015). The Sol-gel Handbook part one. In D. L. Zayat, *The Sol-gel Handbook* (pp. 3-27). Weinheim: Wiley-VCH.

Znaidi, L. (2010). Sol-gel deposited ZnO thin films: A review. *Material Science and Engineering B*.